Journal of Hydrology 563 (2018) 909–926

Contents lists available at ScienceDirect

Journal of Hydrology

journal homepage: www.elsevier.com/locate/jhydrol

Research papers

The response of crop water productivity to climatic variation in the upper-middle reaches of the Heihe River basin, Northwest China

Jun Niu[a,*], Qi Liu[a], Shaozhong Kang[a], Xiaotao Zhang[b]

[a] Center for Agricultural Water Research in China, China Agricultural University, Beijing 100083, China
[b] Key Laboratory of Tibetan Environment Changes and Land Surface Processes, Institute of Tibetan Plateau Research, Chinese Academy of Sciences, Beijing 100101, China

ARTICLE INFO

This manuscript was handled by G. Syme, Editor-in-Chief, with the assistance of Bellie Sivakumar, Associate Editor

Keywords:
SWAT model
Crop yield
Crop water productivity
Climatic variation
Wavelet coherence
Northwest China

ABSTRACT

The Heihe River basin is one of the important bases for commercial grain production in China. The climate change impacts on crop yield and crop water productivity (CWP) need to be examined for sustainable development of regional agriculture, especially under the pressure of population growth and regional water scarcity. A distributed hydrological model was constructed for the upper-middle reaches of the Heihe River basin on the basis of the Soil and Water Assessment Model (SWAT). The sensitivity ranks of hydrological parameters were evaluated for the runoff and evapotranspiration processes, and then independently calibrated with the observations of three gauging stations (Qilian, Zhamashike, and Yingluoxia stations) and the evapotranspiration data derived by remote-sensing. The study first simulated crop yield and CWP for four typical crop types, namely corn, spring wheat, spring barley, and spring canola-Polish, for the period of 1966–2014 using the SWAT model, calibrated with the crop yield data (during the period of 2005–2014) from Zhangye Statistics Yearbook. The spatial-temporal features of crop yield and CWP were analyzed. A fluctuating growth was found for the 49 year trend of corn, spring wheat, and spring canola-Polish. The spring barley shows a slightly decreasing trend. The high-yield area moved from the west part (Suzhou and Gaotai counties) to the east part (Linze, Ganzhou, and Shandan counties) of the basin for the past 49 years, and the area of high CWP concentrated in the Gaotai and Linze Counties. The responses of CWP to climatic forcing were further studied using wavelet coherence method. It is found that maximum temperature dominated the CWP evolutions, especially at the long-term scales. The corn showed the largest elastic responses to the climatic factors, which may be favorable to improve regional CWP by expanding planting area. In addition, the strategies of regional CWP improvement were discussed based on the results.

1. Introduction

China's food production is one of fundamental issues of China sustainability development, and the food security is the most important concern in national agricultural development (Jiang, 2014; Wang et al., 2017). With the population growth, the sustainable agriculture development is further challenged by water scarcity (Saeigs and van Berkel, 1995; Heilig et al., 2000; Wallace et al., 2002). Meanwhile, the climate change has exerted its effects on natural and human systems (Wang et al., 2009; Nguyen et al., 2010; Sivakumar, 2011). Correspondingly, the crop growth has been affected, even some decrease of crop production is observed (IPCC, 2014). Therefore, under the challenging environment of both climate and water shortage, whether we can keep the level of crop production, whether we can reduce the agricultural water requirement under the current production level, and whether we can increase crop yield under current water consumption level, are the critical issues of the sustainable agricultural water management and food security in China.

The Heihe River basin in Northwest China (see Fig. 1) is one the major commercial grain bases, and relies on agriculture economy. The water usage for irrigated agricultural is about 80% of the total water consumption (Zhang et al., 2006), and the percentage is still increasing. This intensified the conflicts between the agricultural water use in the middle reaches and the ecological water use in the lower reaches. To guarantee the regional food security and relieve the contradiction, it is essential to improve the regional crop water productivity (CWP), which is defined as the crop yield over the water use by actual evapotranspiration (Kajine et al., 2003).

The CWP reflects the returned benefits by the consumed water, which is of great importance in agricultural production (Bouman, 2007). The factors affecting CWP are mainly divided into two categories, climate factors and management factors. The management

* Corresponding author.
E-mail address: niuj@cau.edu.cn (J. Niu).

https://doi.org/10.1016/j.jhydrol.2018.06.062
Received 14 January 2018; Received in revised form 25 April 2018; Accepted 24 June 2018
Available online 28 June 2018
0022-1694/ © 2018 Elsevier B.V. All rights reserved.

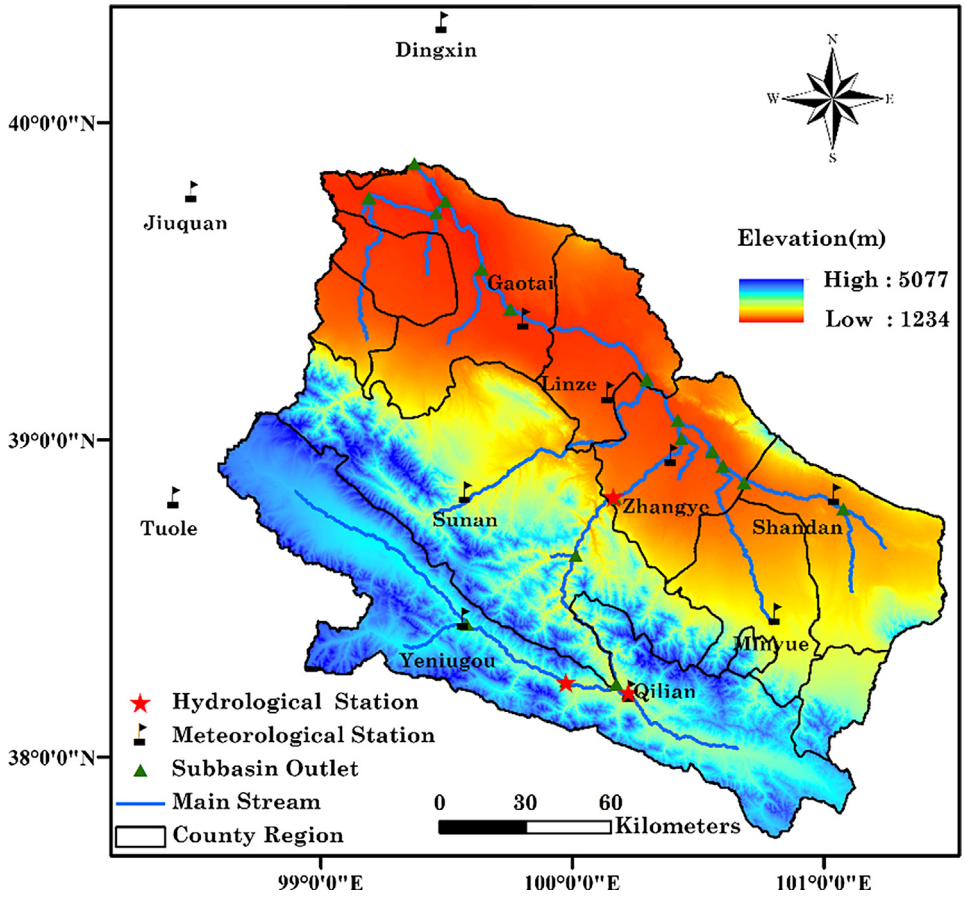

Fig. 1. The meteorological/hydrological stations, and sub-basins, in the Heihe River basin in the Northwest China. The background is the DEM in 30 m spatial resolution obtained from the Data Management Center of the Heihe Research Program (http://www.heihedata.org).

includes both crop and agricultural management. A better understanding of the factors, and their contributions to historical yield and CWP increase, is significant to predict the future trend. Sacks and Kucharik (2011) employed the Agro-IBIS agroecosystem model with the 25-year observations to investigate the effects of crop management (changing planting dates and crop growing degree day requirements) on crop yields (the major component of CWP). Among it, agricultural management includes fertilization and irrigation activities. Irrigation affects CWP mainly through the crop yield and evapotranspiration (Siebert and Doll, 2010). There are already many studies for optimizing irrigation schedules to improve reginal CWP (Zhang and Oweis, 1999; Liu et al., 2004; Xue and Ren, 2017). However, the responses of CWP to regional climate variations are seldom studied and reported. The underlying mechanism is that the warming climate may alter the crop water requirement, through affecting the photosynthesis and respiration processes, and then influences crop yield and evapotranspiration (Zhao et al., 2010; Feng, 2014; Zhang et al., 2015), resulting in regional CWP evolutions. Meanwhile, agrometeorological hazards and primary cropping patterns, which are affected by climatic changes, also lead to variations in crop yield and CWP (Zhou, 2012; Wen et al., 2017; Wang et al.,2017).

The intensified climate evolutions, with increased temperature and changing precipitation amount, for the Heihe River basin has been reported in the study of Wang and Zhang (2010) and Cao et al. (2003) for recent 50 years. The effects of climate changes on CWP cannot be ignored, especially for the water-shortage area of Northwest China. The historical changes are need to be assessed, to identify the spatial-temporal features of CWP and its trend, to find the regional water-saving potentials, and to form reasonable water allocation schemes (Singh et al., 2006; Liu et al., 2007; Faramarzi et al., 2010). The regulation and improvement of CWP is an inevitable way to relieve water-shortage problem, to improve national food security for a sustainable development of agriculture in China. The long-term crop yield data for a large-scale basin is usually limited. Soil and Water Assessment Tool (SWAT) model has been proven to be useful tool to simulate the hydrological cycle and crop growth simultaneously (Arnold et al., 1998; Wu et al., 2012). The suitability of SWAT simulation crop yield and spatial-temporal distribution of CWP has been reported (Arnold and Allen, 1996; Immerzeel et al., 2008; Luo et al., 2008; Schuol et al., 2008; Setegn et al., 2010). Sun and Ren (2014) studied the effects of different irrigation scenarios on the crop yield and CWP in the Haihe River basin in North China. The simulations of hydrological processes in the Heihe River basin in Northwest China using SWAT model were also reported (Zhang et al., 2016; Yang et al., 2017). For example, the evapotranspiration changes in one part of Heihe agricultural region were examined using remotely-sensed ET data and with the SWAT model in study of Zou et al. (2017). These studies all support the utilization of SWAT model on the simulations of the spatial-temporal distributions of CWP over the upper-middle reaches of the Heihe River basin.

On the basis of previous studies, this study attempted to construct a distributed hydrological model for crop yield and CWP simulations over the upper-middle reaches of the Heihe River basin for the period of 1966–2014 using the SWAT model. The model is well calibrated and validated, and the evapotranspiration and yields of four main crops are assessed in details in our study. Then, the long-term spatial-temporal features of crop yield and CWP were discussed and evaluated. Overall, this paper aimed at investigating the effects of different meteorological factors on CWP at the regional scale of Heihe River basin. This paper is organized as follows: Section 2 introduces the Heihe River basin in Northwest China. Section 3 provides the briefs of SWAT model, model

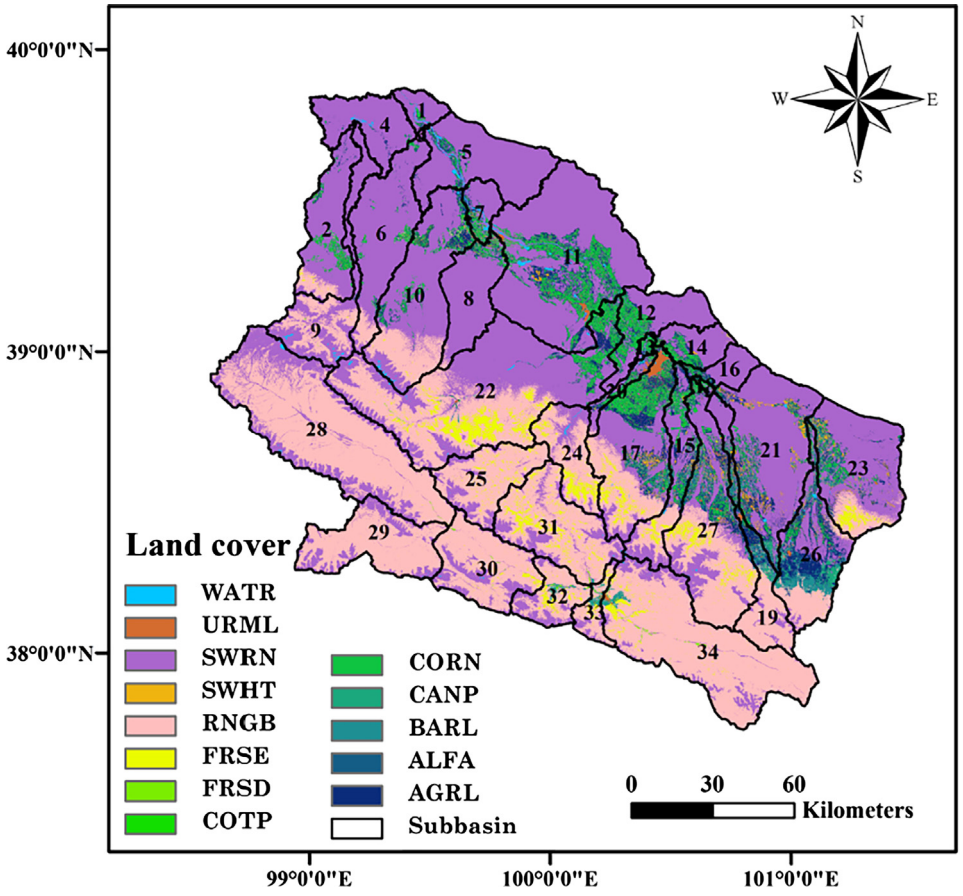

Fig. 2. Land use map of the upper-middle reaches of the Heihe River basin.

Table 1
Data of geography, climate and agricultural management used for model setup and calibration.

Data type	Date description	Source
Digital elevation model	30 m × 30 m resolution	Heihe Plan Science Data Center
Land use map	1:100000 scale, 13 basic land cover categories	Heihe Plan Science Data Center
Soil map	1:1500000 scale, 43 soil types	Heihe Plan Science Data Center
Soil characteristics	Properties were quantified based on measurements or estimated using MATLAB, SPAW software and EXCEL	Gansu soil statistics yearbook
Meteorological data	Daily precipitation, temperature, relative humidity, wind speed of eleven meteorological station located in and around study area (1964–2014)	Heihe Plan Science Data Center
Agricultural management	Crop planting, irrigation and fertilization scheduling	Zhangye Statistics Yearbook
Remote sensing ET	1 km × 1 km resolution, monthly scale, ETWatch model simulation (2000–2013)	Heihe Plan Science Data Center
Crop yield	The annual average crop yield (2005–2014)	Zhangye Statistics Yearbook

Table 2
Land use types in the upper-middle reaches of the Heihe River basin.

Land use types	SWAT code	Area (km^2)	Proportion(%)
Water	WATR	111	0.35
Range-Brush	RNGB	11,066	34.28
Rural residential	URML	169	0.53
Spring Barley	BARL	426	1.32
Spring Wheat	SWHT	223	0.69
Corn	CORN	1626	5.04
Spring Canola-Polish	CANP	119	0.37
Alfalfa	ALFA	70	0.22
Upland Cotton-harvested with picker	COTP	3	0.01
Agricultural Land-Generic	AGRL	1517	4.70
Forest-Deciduous	FRSD	27	0.08
Forest-Evergreen	FRSE	755	2.34
Southwestern US (Arid) Range	SWRN	16,168	50.08

inputs, parameter sensitivity, calibration, and validation. Section 4 presents the results of spatial-temporal features of regional CWP and responses to climate variations. Section 5 concluded the study with a discussion of possible CWP improvement strategies.

2. Study area

The Heihe River (see Fig. 1) is located in the middle of the Hexi Corridor, between 97°42′~102°04′E and 37°41′~42°42′N, which is the second largest inland river in China (Feng et al., 2004). The upper reaches of the Heihe River belongs to the Qilian mountain area, with the elevation between 1680 m and 5280 m and the length of mainstream about 303 km. The middle reaches include a large area of alluvial fans between the Yingluoxia and Zhengyixia stations, with the elevation between 1300 m and1680 m and main stream of about 185-km main stream. The lower reaches of the Heihe River basin is dominated by desert and Gobi.

Table 3
The results of parameter sensitivity analysis for streamflow simulation using the observed data in the three gauging stations.

Parameter[a]	Definition	t-stat[b]	p-value[c]
v_ _SFTMP.bsn	Snowfall temperature (°C)	−5.46	0.00
v_ _SMTMP.bsn	Snow melt base temperature (°C)	3.90	0.00
v_ _CANMX.hru	Maximum canopy index	−3.03	0.00
r_ _CN2.mgt	SCS runoff curve number for moisture condition II	2.65	0.01
v_ _REVAPMN.gw	Threshold depth of water in the shallow aquifer required for "revap" to occur (mm)	−2.03	0.05
v_ _CH_N2.rte	Manning coefficient for channel	−1.94	0.06
v_ _TIMP.bsn	Snow pack temperature lag factor	−1.42	0.16
v_ _SMFMN.bsn	Minimum melt rate for snow during the year (mm/°C/day)	1.30	0.20
v_ _GWQMN.gw	Threshold depth of water in the shallow aquifer required for return flow to occur (mm)	1.08	0.28
v_ _ESCO.hru	Soil evaporation compensation factor	−1.05	0.30
v_ _GW_DELAY.gw	Groundwater delay times (days)	−0.96	0.34
r_ _HRU_SLP.hru	Average slope steepness	0.92	0.36
v_ _ALPHA_BF.gw	Baseflow alpha factor (days)	−0.85	0.40
v_ _CH_K2.rte	Effective hydraulic conductivity in main channel aluvium (mm/h)	0.83	0.41
r_ _SOL_K.sol	Saturated hydraulic conductivity of first layer (mm/h)	0.78	0.44
r_ _SOL_ZMX.sol	Maximum rooting depth of soil profile	0.71	0.48
v_ _SURLAG.bsn	Surface runoff lag time (days)	−0.50	0.62
v_ _GW_REVAP.gw	Groundwater "revap" coefficient	−0.44	0.66
v_ _EPCO.hru	Plant uptake compensation factor	0.42	0.68
v_ _TLAPS.sub	Temperature lapse rate (°C/km)	0.40	0.69
v_ _SMFMX.bsn	Maximum melt rate for snow during the year (mm/°C/day)	−0.39	0.70

[a] v_ _: parameter value varied according to an absolute change; r_ _: parameter value varied according to relative change.
[b] t-stat indicates parameter sensitivity: the large the t-stat, the more sensitive the parameter
[c] p-value indicates the significance of the t-value: the smaller the p-value, the less chance of a parameter being accidentally assigned as sensitive.

Table 4
The results of parameter sensitivity analysis for evapotranspiration processes.

Parameter[a]	Definition	t-stat[b]	p-value[c]
v_ _CANMX.hru	Maximum canopy index	−11.93	0.00
v_ _ESCO.hru	Soil evaporation compensation factor	3.16	0.00
r_ _CN2.mgt	SCS runoff curve number for moisture condition II	2.29	0.02
r_ _SOL_BD.sol	Moist bulk density	2.25	0.03
v_ _ALPHA_BF.gw	Baseflow alpha factor (days)	1.21	0.23
v_ _EPCO.hru	Plant uptake compensation factor	−0.95	0.34
v_ _GW_DELAY.gw	Groundwater delay times (days)	−0.78	0.44
v_ _GW_REVAP.gw	Groundwater "revap" coefficient	−0.57	0.57
v_ _CH_N2.rte	Manning coefficient for channel	0.56	0.58
r_ _SOL_AWC.sol	Soil available water storage capacity (mm H_2O/mm soil)	−0.49	0.62
v_ _GWQMN.gw	Threshold depth of water in the shallow aquifer required for return flow to occur (mm)	0.31	0.75
r_ _OV_N.hru	Manning's "n" value for overland flow	0.30	0.76
r_ _SOL_ZMX.sol	Maximum rooting depth of soil profile	−0.14	0.89
r_ _SOL_K.sol	Saturated hydraulic conductivity of first layer (mm/h)	−0.10	0.92
v_ _CH_K2.rte	Effective hydraulic conductivity in main channel aluvium (mm/h)	0.07	0.94

[a,b,c] Same to Table 3.

The Heihe River basin belongs to continental arid climate. The vegetation in the upper reaches (see Fig. 2) is covered by mountain forest, shrubs, and grasslands, with the long-term average precipitation about 350 mm and average temperature less than 2 °C, which is the runoff generation area. The farmland concentrates in the middle reaches, a flat oasis area. The light and heat resources are abundant in the reaches, with sunshine duration about 3000–4000 h/year and average temperature of 6–8 °C. However, as the limited precipitation (about 140 mm/year), droughts are frequently occurred (Niu et al., 2017). The seasonal variations show the water supply is increased during the period of April-July, and from December to March, it is the dry season. The relative humidity fluctuates within 40–60%.

The middle reaches of the Heihe River basin include Zhangye city and Linze, Minyue, Qilian, Shandan, Sunan, and Suzhou counties. The Zhangye city is also named as "Golden Zhangye", which is one of the ten commercial grain bases in China. About 92.75% farmland concentrates in the middle reaches of the Heihe River basin, consumed about 86.85% water resources in the basin. The main crops are corn, spring wheat, spring barley, and spring canola-Polish. The area of corn is the largest.

Table 5
Parameters selected for streamflow calibration according to the results of sensitivity analysis and the optimized value of the parameter calibration.

Parameter	Range	Hydrologic process	Optimized value
SFTMP[v]	[−20,20]	Snow melt	3.29
SMTMP[v]	[−20,20]	Snow melt	17.67
CANMX[v]	[0,100]	Surface runoff	17.90
CN2[r]	[−0.2,0.2]	Surface runoff	0.19
REVAPMN[v]	[0,500]	Groundwater	92.33
CH_N2[v]	[−0.01,0.3]	Concentration of channel	0.14
TIMP[v]	[0,1]	Snow melt	0.36
SMFMN[v]	[0,20]	Snow melt	4.81
GWQMN[v]	[0,2]	Groundwater	1.27
ESCO[v]	[0,1]	Soil water and soil evaporation	0.09
GW_DELAY[v]	[30,450]	Groundwater	42.51
HRU_SLP [r]	[−0.3, 0.3]	Surface runoff	0.16

[v] Parameter value is replaced by given value.
[r] Parameter value is multiplied by (1 + a given value).

Table 6
Model performance statistics of the simulated and measured streamflow at three gauging stations.

Station	Calibration				Validation			
	Statistical period	NS	E_1	d_r	Statistical period	NS	E_1	d_r
Zhamashenke	1995–1997	0.79	0.72	0.86	1998–2000	0.73	0.62	0.81
Qilian	1995–1997	0.80	0.72	0.86	1998–2000	0.72	0.60	0.80
Yingluoxia	1966–1984	0.76	0.50	0.74	1985–1995	0.74	0.51	0.73

3. Method

3.1. Hydrological modelling

3.1.1. SWAT model

The SWAT model (Arnold et al., 1998) was developed by the United States Department of Agriculture (USDA) in 1994. It is a physical-based, semi-distributed model that applies on a watershed scale. The model can integrate the various spatial data to simulate the hydrological cycles and physical-chemical processes for different watersheds. The sub-basins are delineated for a large-scale river basin based on Digital elevation model (DEM) data and water-collecting area. The hydrologic response unit (HRU) is further derived according to land use and soil types on the basis of sub-basins. The HRU is minimum simulation unit for modelling hydrological and related-processes with the meteorological forcing data and model parameters. The generated runoff is routed to the basin outlet for the estimations of streamflow, sediment and chemical loadings (Neitsch et al., 2005). SWAT is a combination of

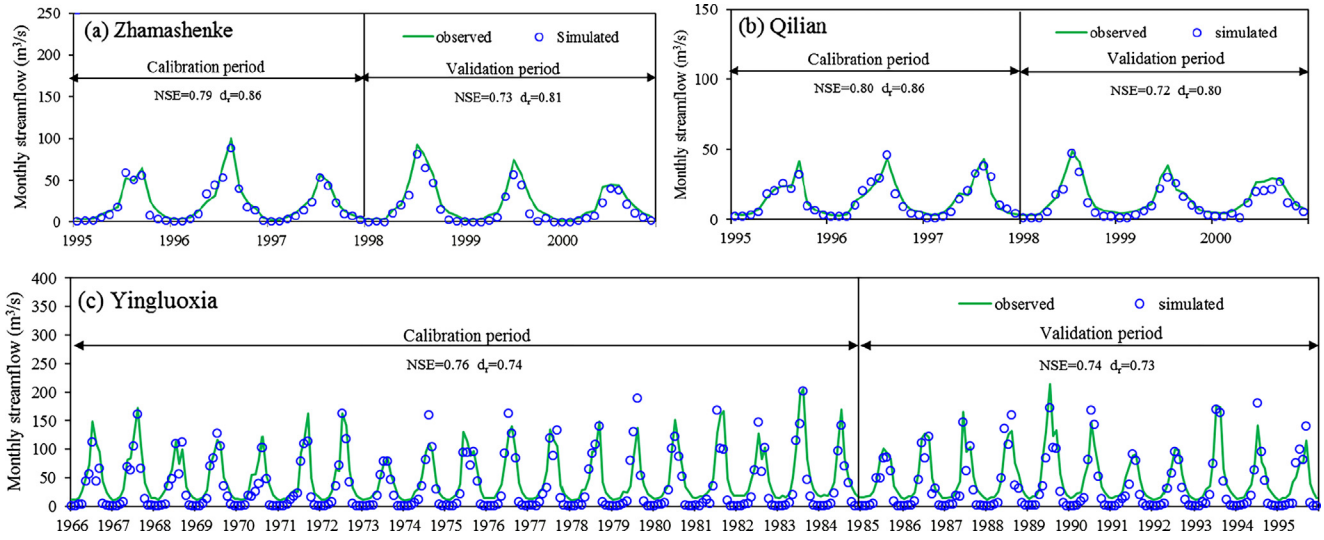

Fig. 3. The simulations and observations of the monthly streamflow at Zhamashenke, Qilian, and Yingluoxia gauging stations.

Table 7
Parameters selected for evapotranspiration calibration according to the results of sensitivity analysis and the optimized value of the parameter calibration using remotely- sensed actual evapotranspiration as the observed data in 34 sub-basins of the Upper-middle reaches of the Heihe River basin.

Parameter[a]	Range	Hydrologic process	Optimized value
CANMX[v]	[0,100]	Surface runoff	0.26
ESCO[v]	[0,1]	Soil water and soil evaporation	0.57
CN2[r]	[−0.2,0.2]	Surface runoff	0.16
SOL_BD[r]	[−0.2,0.2]	Infiltration and soil water	−0.05
ALPHA_BF[v]	[0,1]	Groundwater	0.28
EPCO[v]	[0,1]	Soil water and soil evaporation	0.27
GW_DELAY[v]	[0,500]	Groundwater	98.85
GW_REVAP[v]	[0.02,0.2]	Groundwater	0.11
CH_N2[v]	[−0.01,0.3]	Concentration of channel	0.1
SOL_AWC[r]	[−0.2,0.2]	Infiltration and soil water	−0.24

[v] Parameter value is replaced by given value.
[r] Parameter value is multiplied by (1 + a given value).

different modules, and each hydrological process corresponds to a module. The runoff generation is enabled by the SCS curve or Green-Ampt infiltration module. The SCS curve (USDA-SCS, 1972) is adopted in this study with considering soil penetrability, land cover, and antecedent soil water conditions. The soil water flow is calculated by the dynamic tank method (Sloan et al., 1983) with considering hydraulic conductivity, slope, and spatial-temporal changes of soil water. The river channel routing is realized by the variable-coefficient model or the Muskingum method. The evapotranspiration in the model includes canopy interception, soil evaporation, and plant transpiration. The Penman-Monteith method (Monteith, 1965) is selected in this study to calculate the potential evapotranspiration (PET) with the meteorological data of air temperature, solar radiation, relative humidity, and wind speed. The PET and soil cover index are used to compute the potential soil evaporation. Actual soil evaporation is a function of soil depth and an exponential function of soil water. The actual plant transpiration is a function of PET, soil water content and root depth.

The plant growth in SWAT model is developed based on the Environmental Policy Integrated Calculator (EPIC) crop model (Williams et al., 1984). The daily variations of the leaf area index, canopy height, and root growth are simulated based on the radiation-derived potential growth. The biomass increase for a given day is estimated based on the photosynthetically active radiation and the plant radiation-use efficiency. Then the crop yield is calculated based on the above ground biomass and harvest index.

3.1.2. Data input and model setup

The Digital elevation model (DEM) data used in this study is provided by Heihe Plan Science Data Center (http://heihedata.org/) with the spatial resolution of 30 m, from which the basin boundary and its stream network are extracted. The relevant geophysical information, such as slope and stream length, are also calculated by the DEM data. The upper-middle reaches of the Heihe River basin was finally discretized into 34 sub-basins, in which the upper reaches include 9 sub-basins mainly in Qilian and Sunan Counties, and the middle reaches include 25 sub-basins mainly distributed in Gaotai, Linze, Ganzhou, Minyue, and Sandan Counties. Other required data needed for model setup and the data sources are listed in Table 1.

The distributions of different soil types for the studied region are obtained from the vectorization map with the scale of 1:15000000. The soil properties are mainly described as physical and chemical parameters, which were quantified based on field measurements or estimated using statistical methods. The land use data is interpreted from landsat remotely-sensed data, with a spatial resolution of 30 m, obtained from Heihe Plan Science Data Center. The 13 land use types are listed in Table 2. The farmland area occupied about 40.8% in the middle reaches, with crops of corn, spring wheat, spring barley, and spring canola-Polish. Meanwhile, there are a small part of farmland, located between Zhamshke and Qilian stations, in the upper reaches of the basin, where the crops are mainly spring barley and spring canola-Polish. The land use, soil and slope datasets were linked with the SWAT databases and 49 sub-basins were further subdivided into 1613 HRUs.

The meteorological data were also obtained from the Heihe Plan Science Data Center. The climate data at 11 stations (Qilian, Sandan, Mingyue, Sunan, Yeliugou, Linze, Gaotai, Jiuquan, Dingxin, and Tuole) for the period of 1964–2014 were used in the SWAT model. The data includes daily precipitation, the maximum and minimum temperature, relative humidity, and solar radiation. The period of 1964–1966 was set as spin-up period.

3.1.3. Sensitivity analysis, model calibration and validation

The sensitivity analysis, parameter uncertainty analysis and calibration in this study are accomplished by Sequential Uncertainty Fitting (SUFI-2) using the SWAT-CUP program (Abbaspour et al., 2004, 2007). In SUFI-2, the parameter uncertainty considers all sources of uncertainties, including uncertainty in driving variables, in the conceptual model, in model parameter, or the observed data. The 95% prediction uncertainty (95PPU) is employed to quantify the uncertainty in the output caused by the parameter uncertainty. The effectiveness of the calibration-uncertainty is reflected by two indices, P-factor and R-

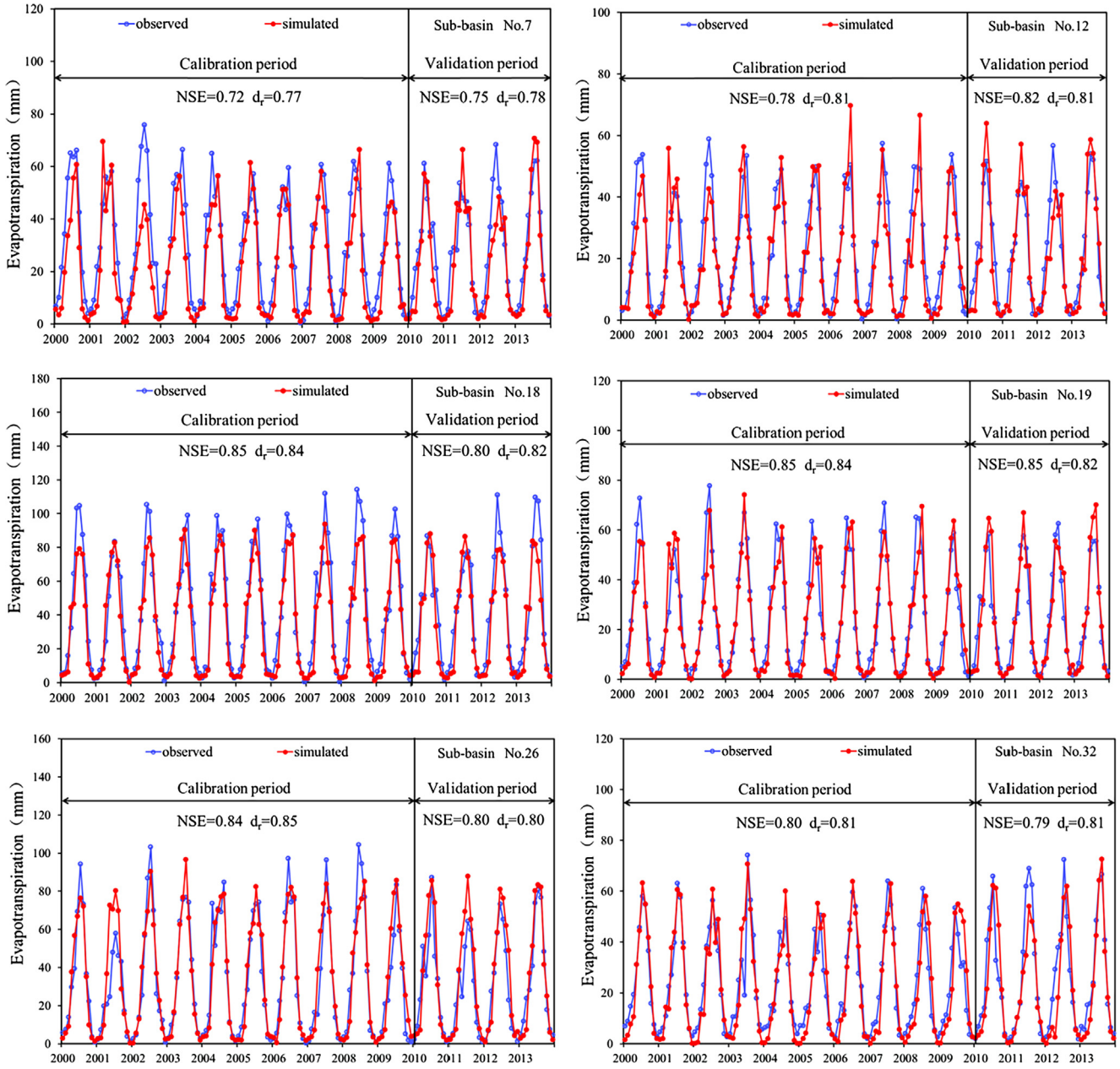

Fig. 4. The simulations and observations of the monthly evapotranspiration at six representative sub-basins of the calibration period (2000–2009) and the validation period (2010–2013).

Table 8
Model performance statistics of the simulated and observed evapotranspiration in six representative sub-basins.

Sub-basin	Calibration period (2000–2009)			Validation period (2010–2014)		
	NS	E_1	d_r	NS	E_1	d_r
No. 7	0.72	0.55	0.77	0.75	0.56	0.78
No. 12	0.78	0.62	0.81	0.82	0.61	0.81
No. 18	0.85	0.68	0.84	0.80	0.64	0.82
No. 19	0.85	0.68	0.84	0.85	0.64	0.82
No. 26	0.84	0.71	0.85	0.80	0.61	0.80
No. 32	0.80	0.62	0.81	0.79	0.62	0.81

factor. P-factor is the percentage of measured data bracketed by the 95PPU band, while R-factor is the average width of the band divided by the standard deviation of the corresponding measured variable. P-factor approaching to 1 and R-factor approaching to 0 are the ideal situation to bracket most of the measured within the 95 PPU band. In addition to the common objective functions of Nash-Sutcliffe (NS), mean relative error (MRE), relatively root mean square error (RRMSE), relative bias index (PBIAS), two other indices representing more interpretable class of measures based on the sum of error magnitudes are used, which are E_1 and d_r (Willmott et al., 2011) to determine the performance of the model, which are given as:

$$NS = 1 - \frac{\sum_{i=1}^{n} (Q_{o,i} - Q_{s,i})^2}{\sum_{i=1}^{n} (Q_{o,i} - \overline{Q_o})^2} \quad (1)$$

$$MRE = \frac{\sum_{i=1}^{n} |[(Q_{s,i} - Q_{o,i})/Q_{o,i}]|}{n} \quad (2)$$

Table 9
Calibration results of the four main crop parameters.

Parameter	Description	CORN	SWHT	BARL	CANP
BIO_E	Radiation use efficiency (kg/ha)/(MJ/m^2)	40	37	35	34
HVSTI	Harvest index	0.55	0.57	0.49	0.28
BLAI	Maximum potential leaf area index	6.5	3.5	3	3
FRGRW1	Fraction of plant heat unit at point 1	0.15	0.15	0.15	0.15
LAIMX1	Fraction of leaf area index at point 1	0.05	0.05	0.01	0.02
FRGRW2	Fraction of plant heat unit at point 2	0.5	0.5	0.45	0.45
LAIMX2	Fraction of leaf area index at point 2	0.95	0.95	0.95	0.95
DLAI	Fraction of plant heat unit when LAI begins to decline	0.8	0.65	0.5	0.6
T_BASE	The base temperature of plant growth	9	0	0	4
GSI	Maximum stomatal conductance (m/s)	0.01	0.004	0.007	0.006
EXT_COEF	Light extinction coefficient	0.65	0.55	0.6	0.65
CHTMX	Maximum canopy height (m)	2.7	1.3	1.4	0.7

$$RRMSE = \sqrt{\frac{\sum_{i=1}^{n}(Q_{o,i}-Q_{s,i})^2}{n}} \Big/ \overline{Q_o} \tag{3}$$

$$PBIAS = \frac{\sum_{i=1}^{n}(Q_{s,i}-Q_{o,i})}{\sum_{i=1}^{n} Q_{o,i}} \tag{4}$$

$$E_1 = 1-\frac{MAE}{MAD} = 1-\frac{\sum_{i=1}^{n}|Q_{s,i}-Q_{o,i}|}{\sum_{i=1}^{n}|Q_{o,i}-\overline{Q_o}|} \tag{5}$$

$$d_r = \begin{cases} 1-\frac{MAE}{2\cdot MAD} = 1-\frac{\sum_{i=1}^{n}|Q_{s,i}-Q_{o,i}|}{2\sum_{i=1}^{n}|Q_{o,i}-\overline{Q_o}|}, & \text{when } \sum_{i=1}^{n}|Q_{s,i}-Q_{o,i}| \leqslant 2\sum_{i=1}^{n}|Q_{o,i}-\overline{Q_o}| \\ \frac{2\cdot MAD}{MAE}-1 = \frac{2\sum_{i=1}^{n}|Q_{o,i}-\overline{Q_o}|}{\sum_{i=1}^{n}|Q_{s,i}-Q_{o,i}|}-1, & \text{when } \sum_{i=1}^{n}|Q_{s,i}-Q_{o,i}| > 2\sum_{i=1}^{n}|Q_{o,i}-\overline{Q_o}| \end{cases} \tag{6}$$

where $Q_{o,i}$ stands for the observed streamflow value, $Q_{s,i}$ represents simulated value, $\overline{Q_o}$ is the average value of observations, $\overline{Q_s}$ is the mean value of simulation, and n is the number of time positions.

In general, sensitivity analysis is an indispensable step to identify parameters to be calibrated. The sensitivity analysis adopted in this study is the Latin hypercube one-factor-at-a-time (LH-OAT) method (van Griensven et al., 2006). Twenty-one hydrological parameters were selected in the sensitivity analysis for the simulation of the streamflow. The data for period 1995–1997 were used for sensitivity analysis and calibration, while the data from 1998 to 2000 were choosed for model validation in both Qilian gauging station and Zhamashenke gauging station. In Yingluoxia gauging station, there were longer term series data for calibration and validation, which were period 1966–1984 and period 1985–1995, respectively. As the ET is requisite for the CWP calculation, fifteen parameters were selected for the sensitivity analysis and calibration in processing ET data. The ET data was obtained from the Data Management Center of the Heihe Research Program (http://westdc.westgis.ac.cn/) with a spatial resolution 1 km for the period of 2000–2013. The 2000–2009 and 2010–2013 are the calibration and validation period respectively.

The crop growth simulation is directly related to the crop yield and ET process during the growing season. Therefore, it is also critical to calibrate the relevant parameters for the growing period. The long-term crop yield can mainly fall into trend yield (which is considered as the result of agricultural investment and technology development) and climatic fluctuant yield (which is considered as the contribution of climatic variations) (Fang, 2011). By employing the five-point moving average method, the detrending crop yield was obtained with the yield

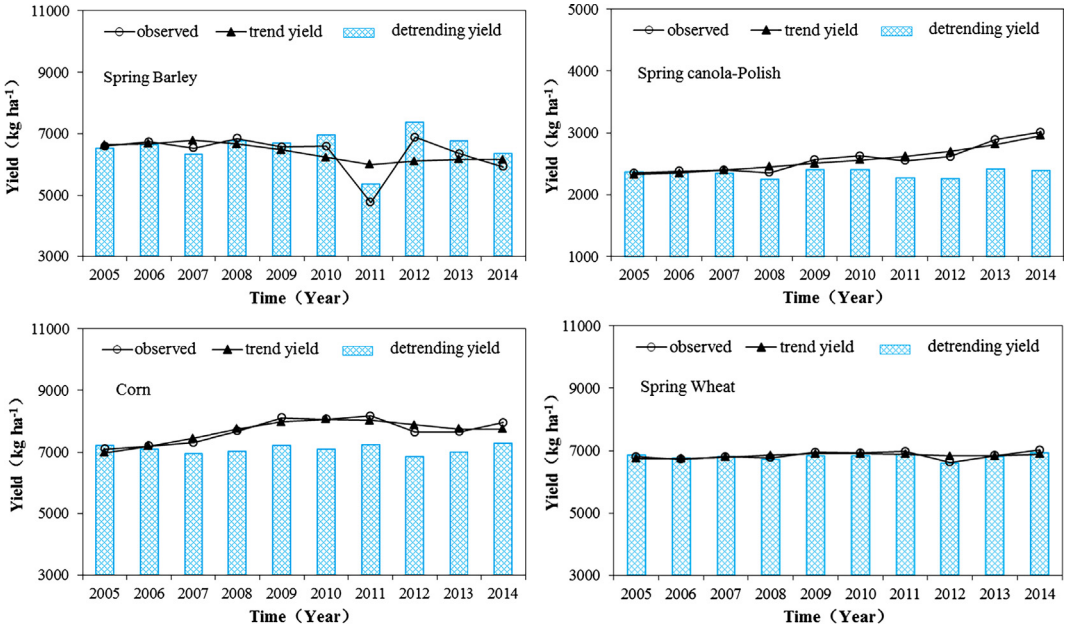

Fig. 5. Detrending crop yield for the four typical crops during 2005–2014 in the upper-middle reaches of the Heihe River basin.

Table 10
Model performance statistics of the climatic fluctuant yield and simulated yield of four main crops at six counties.

Region	BARL			CORN			SWHT			CANP		
	PBIAS	RRMSE	MRE	PBIAS	RRMSE	MRE	PBIAS	RRMSE	MRE	PBIAS	RRMSE	MRE
Ganzhou	0.15	0.27	26.51	−0.01	0.10	8.71	−0.02	0.13	10.87	—	—	—
Gaotai	0.15	0.21	16.20	0.01	0.15	11.29	−0.06	0.14	11.05	—	—	—
Linze	2.34	0.08	13.42	0.01	0.12	11.57	0.04	0.13	12.27	—	—	—
Minyue	−0.04	0.26	20.58	0.04	0.16	12.95	0.01	0.15	10.84	−0.07	0.12	6.74
Shandan	0.00	0.22	14.46	−0.04	0.14	11.86	−0.02	0.16	12.35	0.03	0.06	5.28
Sunan	0.11	0.18	11.24	0.04	0.17	16.38	0.31	0.36	29.33	0.06	0.30	20.46

Note: '—'means no statistic result at the county region due to the lack of simulated data.
PBIAS, relative bias index; RRMSE, mean relatively root mean square error; MRE, mean relative error (%).

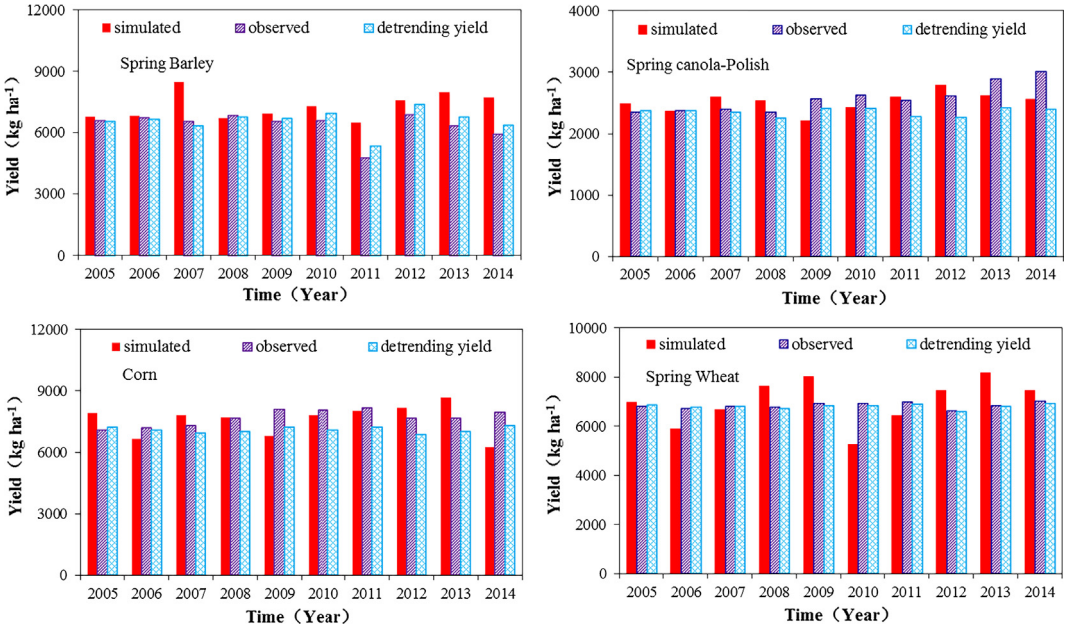

Fig. 6. Comparisons of the simulated crop yield, detrending yield and the statistical data obtained from Zhangye Statistics Yearbook for the four typical crops during 2005–2014 in the upper-middle reaches of the Heihe River basin.

Table 11
Summary of trend analysis for crop yield, CWP, and meteorological factors using the Mann-Kendall nonparametric test.

Variable		Mean value	Zs	Trend	Significance
Yield	Total	5739.04	6.46	↗	***
	CORN	5797.52	6.04	↗	***
	BARL	7844.23	−0.8	↘	—
	SWHT	5420.35	5.61	↗	***
	CANP	2111.73	5.99	↗	***
Crop Water Productivity	Total	1.26	6.25	↗	***
	CORN	1.30	6.06	↗	***
	BARL	1.44	−1.55	↘	**
	SWHT	1.00	5.13	↗	***
	CANP	0.48	5.23	↗	***
Evapotranspiration		453.32	2.42	↗	***
Maximum Temperature		23.70	5.18	↗	***
Minimum Temperature		8.18	6.89	↗	***
Precipitation		109.02	0.30	↗	—
Solar radiation		3100.00	0.00	↘	—
Relative humidity		0.48	−3.27	↘	***
Wind speed		2.36	−2.66	↘	***

Zs: the test statistic in Mann-Kendall nonparametric test.
Trend: ↗ indicates an increase; ↘ indicates a decrease. — Trends are not significant.
Significance: *** Trends are significant at a significance level P ≤ 0.01; ** Trends are significant at a significance level P ≤ 0.05.

data from Zhangye Statistic Yearbook for the period of 2005–2014. The crop yield calibration was performed after calibrating the streamflow and ET for the four crop types, and validated by the detrending crop yields. Twelve parameters were selected in the dominate processes. As the model provides data based on sub-basins, the crop yield is aggregated to the county scale before comparing with the observations.

3.2. Wavelet coherence analysis

Wavelet transform is capable to examine the variability evolution at different timescales, since wavelets display variability in both time and frequency domain (Kumar and Foufoula-Georgiou, 1997; Lau and Weng, 1995). The continuous wavelet transform of a time series x_n (n = 0,..., N–1) is defined as the convolution of x_n with a scaled and translated wavelet $\psi_0(\eta)$,

$$W_n(\xi) = \sum_{\gamma=0}^{N-1} x_\gamma \psi * \left[\frac{(\gamma - n)\delta t}{\xi}\right] \quad (7)$$

where * indicates the complex conjugate, ξ is the wavelet scale for varying the window width as multiples of the lowest frequency ($1/\delta t$, in which δt is the time interval), and γ is the translation parameter to shift the wavelet along the time. The mother wavelet (i.e., Morlet wavelet in this study), $\psi_0(\eta)$, that depends on a non-dimensional 'time' parameter η, is defined as follows (Torrence and Compo, 1998):

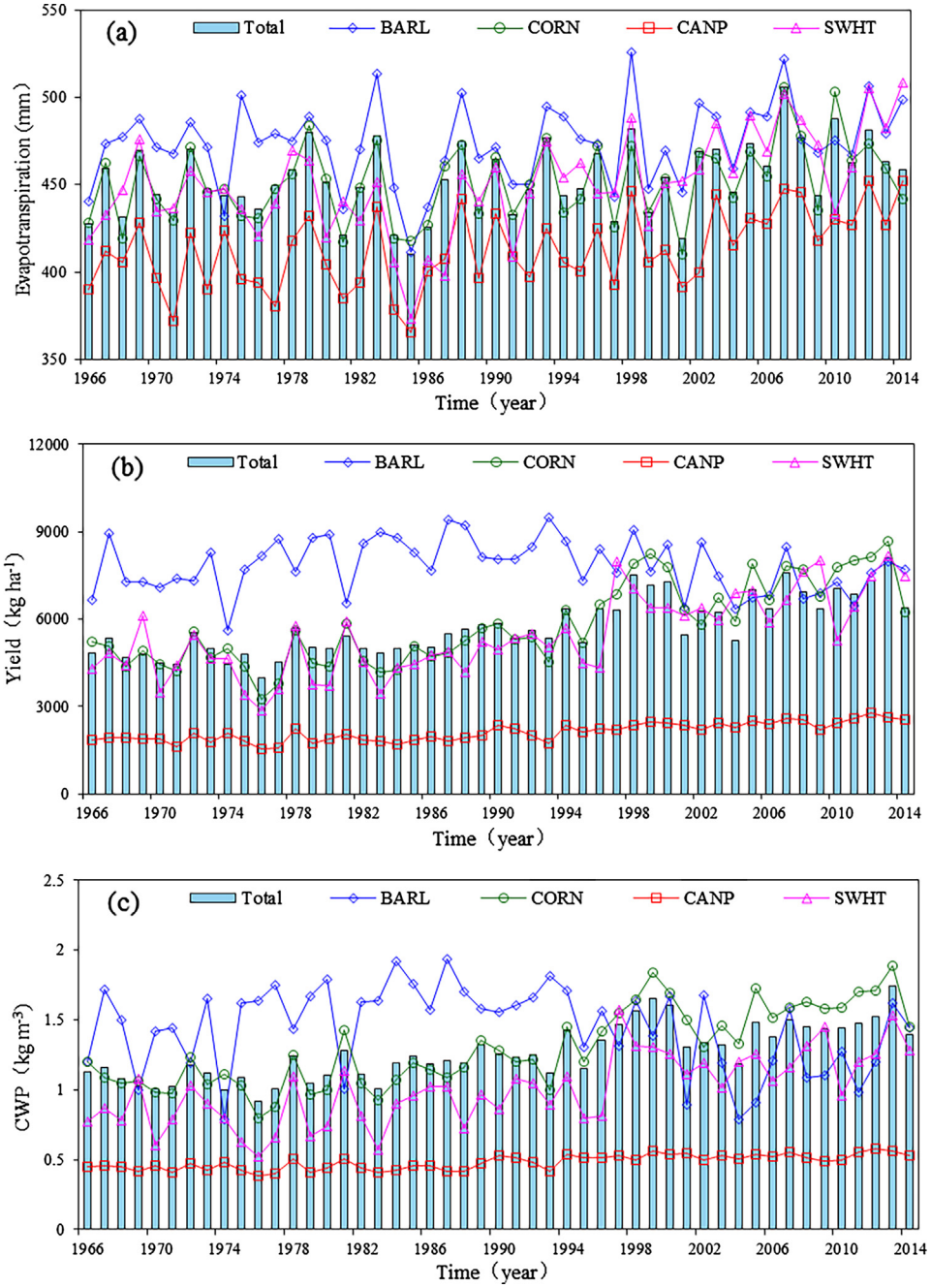

Fig. 7. Changes of crop yield and CWP of spring barley (BARL), spring canola-Polish (CANP), corn (CORN) and spring wheat (SWHT) in the upper-middle reaches of the Heihe River basin during 1966–2014.

$$\psi_0(\eta) = \pi^{-1/4} e^{i\omega_0 \eta} e^{-\eta^2/2} \tag{8}$$

where $\omega_0$is the non-dimensional frequency. The local wavelet power spectrum is defined as $|W_n(\xi, \gamma)|^2$, which gives a local measure of the variance of the analyzed time series at each scale and at each time.

The wavelet coherence analysis is to identify regions in time frequency domain where the two time series co-vary. Following Torrence and Webster (1998), the coherence phase is defined as $\tan^{-1}$[imaginary part of $\{W_n^{XY}(s)\}$/real part of $\{W_n^{XY}(s)\}$], and the wavelet coherence of the two time series is given as follows:

$$R_n^2(s) = \frac{|S(s^{-1} W_n^{XY}(s))|^2}{S(s^{-1}|W_n^X(s)|^2) \cdot S(s^{-1}|W_n^Y(s)|^2)} \tag{9}$$

where S is a smoothing operator, given by (Grinsted et al., 2004):

$$S(W) = S_{scale}(S_{time}(W_n(s))) \tag{10}$$

where S_{scale} is the smoothing along the wavelet scale axis and S_{time} is the smoothing in time. A suitable smoothing operator for the Morlet wavelet is provided by Torrence and Webster (1999) as follows:

$$S_{time}(W)|_s = \left(W_n(s) * c_1^{\frac{-t^2}{2s^2}} \right) \Big|_s \tag{11}$$

$$S_{scale}(W)|_n = (W_n(s) * c_2 \prod (0.6s))|_n \tag{12}$$

where c_1 and c_2 are normalization constants, and $\prod$ is the rectangle function. The factor 0.6 is the decorrelation length of empirically determined scale for the Morlet wavelet (Torrence and Compo, 1998).

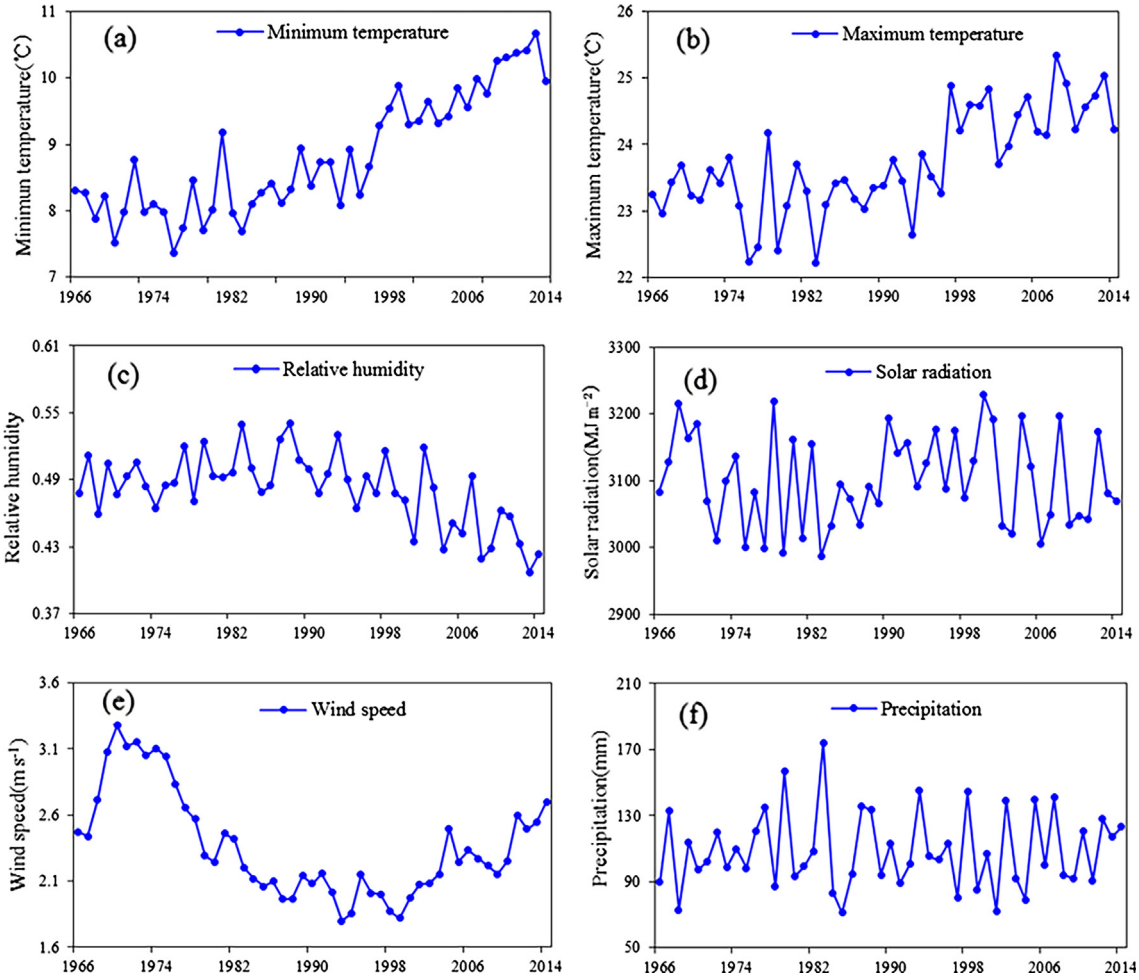

Fig. 8. Changes of mean minimum temperature (a), maximum temperature (b), relative humidity (c), solar radiation (d), wind speed (e) and precipitation (f) during the crop growing seasons for the period of 1966–2014 in the upper-middle reaches of the Heihe River basin.

4. Results

4.1. Sensitivity analysis

The sensitivity analysis was performed for identifying the most sensitive parameters in hydrological and crop-production processes of the SWAT model, as most of them were difficult to obtain by measurement. The sensitivity results for the streamflow processes is listed in Table 3. The t-stat stands for the sensitivity degree. The larger its absolute value, the more sensitive the parameter. The p-value represents the significance of t-value. If the value is closer to 0, the less chance will have for a parameter being accidently assigned as the sensitive one. The ranking of model parameters indicates that the 12 parameters are to be calibrated: SMTMP, CANMX, CN2, REVAPMN, CH_N2, TIMP, SMFMN, GWQMN, ESCO, GW_DELAY, and HRU_SLP. The results of sensitivity study for evapotranspiration are listed in Table 4. The first ten sensitive parameters are CANMX, ESCO, CN2, SOL_BD, ALPHA_BF, EPCO, GW_DELAY, GW_REVAP, CH_N2, and SOL_AWC.

4.2. Model calibration and validation

The streamflow calibration was conducted by SUFI-2 in the SWAT model, with the observations in three gauging stations: Zhamashike, Qilian and Yingluoxia stations. Table 5 provides the range of each parameter and the optimal value after the calibration. The comparisons between the simulated and observed streamflow showed that the calibration results are satisfactory with Nash-Sutcliffe coefficient (NSE) larger than 0.75 and the d_r larger than 0.74. The model was also well performed in the validation period, with NSE larger than 0.70 and d_r larger than 0.73. The results also showed that there are minor differences between the simulated streamflow and observations, with E_1 exceeding 0.5 and d_r up to 0.7. Meanwhile, in the evaluation, P-factor is larger than 0.5 and R-factor is less than 1.0. The detailed calibrated and validated results were listed in Table 6, and graphical comparisons for the monthly streamflow were showed in Fig. 3.

The first ten highly sensitive parameters to ET were calibrated using SUFI-2, based on the validated streamflow simulation. Table 7 listed the initial ranges of each parameter and the respective hydrological process involved. The ET calibration was performed at the 34 sub-basins in the Heihe River basin. The results showed that the P-factor for 73% (i.e. 25/34) sub-basins are large than 0.5. The R-factor for all sub-basins were less than 1.0. Meanwhile, the d_r value for 22 sub-basins were larger than 0.75 and NSE for 19 sub-basins were larger than 0.7. The calibrated model was performed well in the validation period, with the P-factor larger than 0.65 and the R-factor less than 1 for more than 60% of the total sub-basins. In the validation period, there were 22 sub-basins with d_r ranged in 0.60–0.83, 20 sub-basins with NSE larger than 0.73. Fig. 4 and Table 8 illustrated the comparison between the observed and simulated evapotranspiration in several typical sub-basins, and a further demonstration of the model performance was presented in Table 8. The sub-basins 7 and 12 were located in the northwestern part of the Heihe River basin, sub-basins 18, 19 and 26 in the southeastern part, and the sub-basin 32 was in the upper reaches. Meanwhile, the sub-basins 18, 19, and 26 cover a large area of crop lands. The ET

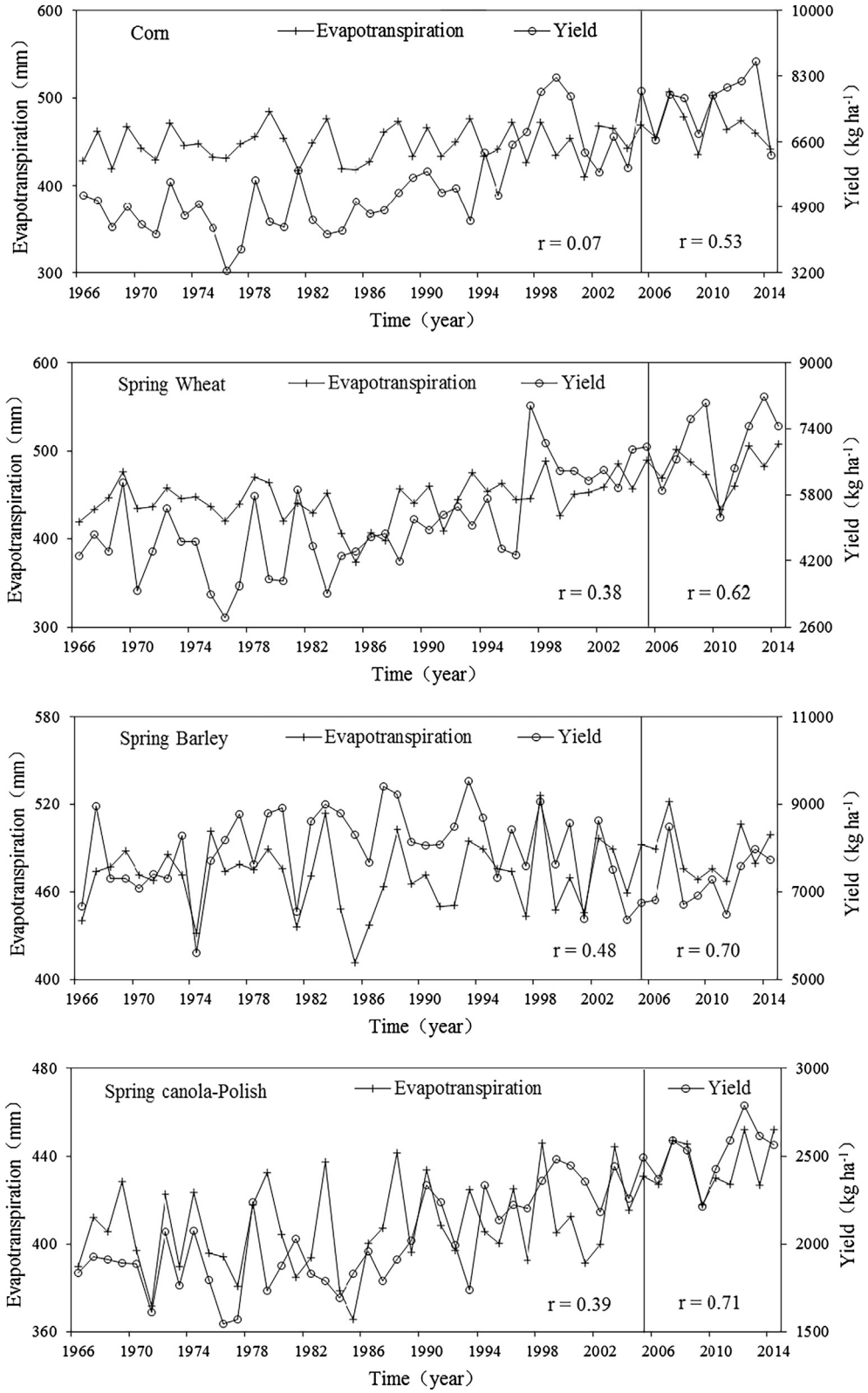

Fig. 9. Comparisons of the crop yield and evapotranspiration for the four main crop in the upper-middle reaches of the Heihe River basin during 1966–2014.

variations over these sub-basins represented characteristics of the regional ET, and the simulated results were in good agreement with the observed data. Overall, the calibrated SWAT model can simulate ET well for the upper-middle reaches of the Heihe River basin.

Table 9 listed the calibrated results of crop parameters for the four crop types (i.e., corn, spring wheat, spring barley, and spring canola-Polish) in the Heihe River basin. Among it, the 6 parameters (FRGRW_1, LAIMX_1, FRGRW_2, LAIMX_2, BLAI, and DLAI) controlled the evolutions of Leaf Area index (LAI) for the crop growing season. During the calibration process, the modified step of the parameters FRGRW_1, LAIMX_1, FRGRW_2, and LAIMX_2 was 0.05, and for BLAI and DLAI were 0.5 and 1 respectively. The BIO_E, HVSTI, and CHTMX, were the

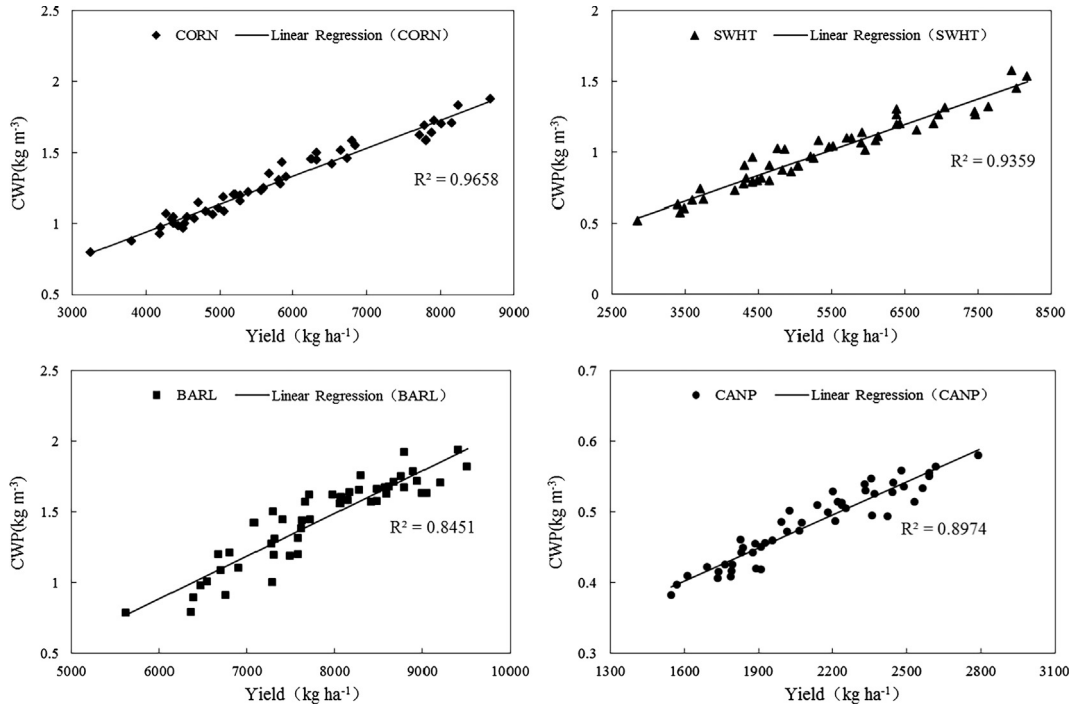

Fig. 10. Relationship between CWP and crop yield for the four main crop of the Heihe basin during 1966–2014.

main control parameters for biomass, crop yield, and height, with the modified step 1, 0.05, and 0.2 respectively. The results showed that the calibrations of harvest index and canopy height optimized the crop yield simulations. The T-BASE and GSI directly affected the length of growing season and ET processes. The final optimum values for the 12 parameters were listed in Table 9.

The statistical measures and graphical comparisons between the simulated crop yield and climatic fluctuant yield (in Fig. 5) were shown in Table 10 and Fig. 6 respectively. The statistics showed that the MRE values for the 6 counties were all less than 25%, and the PBIAS values were basically close to 0. The simulations were not better for spring barely, partly due to the crop is scattered in the region, which increased the collection uncertainty of observed data in the statistical Yearbook. Fig. 6 demonstrated the good agreement for the simulated and observed detrending crop yield over the agricultural region in the Heihe River basin. As the crop yield simulations were calibrated with the data of recent ten years (2005–2014), the crop yield for the first 40 years (1966–2005) were actually based on the agricultural cultivar conditions in recent ten years. Therefore, we stated that the responses of CWP for the studied period is mainly on climatic variations, with the cultivar background of the recent ten years.

4.3. Spatial-temporal features of crop yield and CWP

ET and the crop yield of corn, spring wheat, spring barley, and spring canola-Polish for the period of 1966–2014, over the upper-middle Heihe River basin, were simulated by the calibrated SWAT model. The Mann-Kendall nonparametric test was applied to show the temporal trend of different variables of the whole region and the results are summarized in Table 11. Fig. 7(a) showed that ET had an increase trend with fluctuations between 410 mm (in 1985) and 505 mm (in 2007). Comparing the ET evolutions with the corresponding precipitation in Fig. 8, the fluctuations were closely related, with the correlation value 0.72. Especially, the minimum ET matched the minimum precipitation amount in 1985. Therefore, the precipitation was a main meteorological driving force for the reginal ET. In addition, the values of ET peak occurred more during the period of 1989–2014 with 2–3 years a time than those in the period of 1966–1988 with 4–5 years. During the whole period of 1966–2014, the total crop yield also showed a slowly increasing trend, but the increasing rate was slightly higher during the period of 1990–2014. It is found that the changing trend were similar with that of Maximum/Minimum temperature trend, which indicated the dominate factors for crop production in studied region. Fig. 7(b) provided the historical trend of crop yield for the four typical crops over the total period of 1966–2014. The changing trends were different under different crop types. The spring canola-Polish showed an increasing trend, which were mainly due to that: (1) the growing season was long, however, the required water was limited by the arid climate (Zhang and Li, 2004); and (2) regarding impacts of the temperature, the canola-Polish was tolerant to low-temperature, and it was mainly planted in the Minyue and Shandan counties closed to the mountain area in the upper reaches. The temperature here was relatively low, and the changing was less obvious than in other regions. The responses of the yield of corn and spring wheat to temperature were relatively obvious, with the different increase rates occurred before and after 1990. The changing pattern of spring barley was different with other three crops, which was similar with the RH in Fig. 8(c), with the correlation value 0.69. The larger spring barley yield occurred in 1967, 1993, and 1998 corresponding to the high RH in these years respectively. The barley yield matched RH at the lower values in 1974, 1981, and 1995. Therefore, the barley yield in the Heihe region showed a significant responses to RH at the annual scale.

Fig. 9 showed the co-variability between crop yield and ET for the period 1966–2014. Generally, a relatively higher crop yield corresponds to the large amount of water consumption, and the relationship is stronger during the period of 2005–2014, which can be demonstrated by the correlation coefficients between yield and ET of different crop types. Among it, the co-variability on increasing trend is more obvious for the spring canola-Polish in the later period, with the correlation coefficient up to 0.71. For corn and wheat, ET during 2005–2014 was increased by 4.81% and 8.66% respectively, compared to ET during 1966–2004. Correspondingly, the yield of corn and wheat was increased 41.86% and 39.55% respectively. A certain temperature increase facilitates the photosystems, and the increased precipitation compensated the required water increase for the photosynthesis (Meng

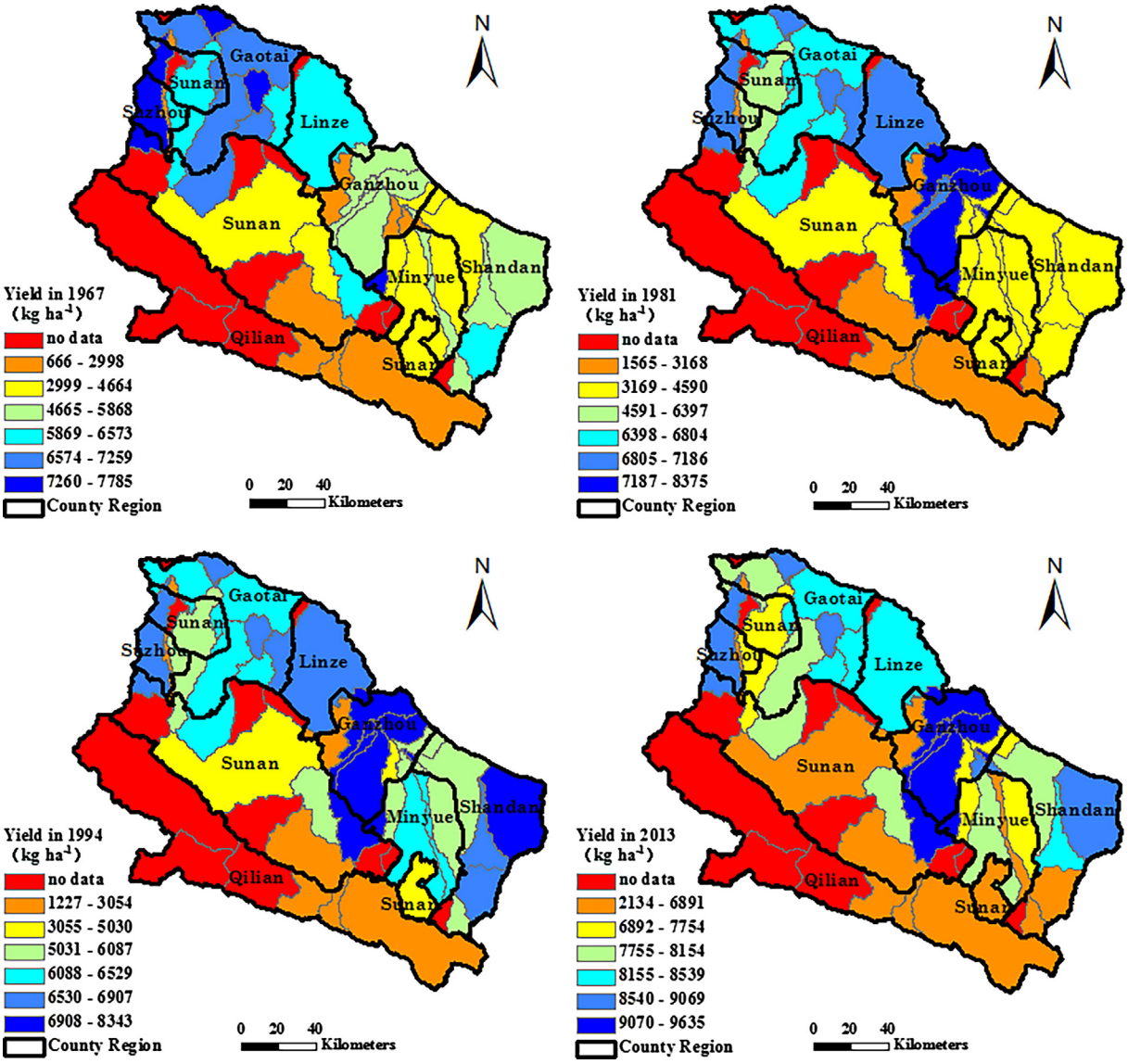

Fig. 11. Simulation results of the average crop yield for the four main crop species in 1967, 1981, 1994, and 2013, respectively.

et al., 2017). Both contributed the consistent changing variations between crop yield and ET evolutions in recent years. But, the spring barley showed a different responses, which indicated ET may not be the dominate factor for the yield.

The CWP evolution was determined by both the changes of ET and crop yield. Fig. 7(c) showed that the total CWP has an increasing trend for the period of 1966–2014. The fluctuation ranged between 0.92 kg m^{-3} and 1.75 kg m^{-3}, corresponding to 3995 kg ha^{-1} in 1967 and 8088 kg ha^{-1} in 2013 respectively. Meanwhile, Fig. 10 demonstrated there is a strong relationship between crop yield and CWP. The R^2 for corn and spring wheat reached 0.97 and 0.94 respectively. This indicated crop yield controlled the CWP evolution in the Heihe River basin.

The changing trend of CWP was different for different crop types. The spring barely had the maximum with the annual average CWP of 1.45 kg m^{-3}. Meanwhile, its CWP variability was also strong, and the CWP reached the lowest in the latter phase in 1996. The long-term average CWP of corn was about 1.30 kg m^{-3}. As has the large proportion of corn yield (i.e. 60% of the total crop yield), the corn CWP had a larger contributions to the evolution of the total CWP in the region. The wheat CWP was relatively lower, with the average value about 1.00 kg m^{-3}. The canola-polish CWP had the lowest CWP with average value of 0.48 kg m^{-3}, which belongs to high water consumption crop, and was mainly planted in Minyue and Shandan counties. Therefore, increasing the corn plant area is a way to improve future regional CWP for the studied region.

The crop planting patterns were different in different counties for the upper-middle reaches of the Heihe River basin. The crop yield and CWP showed spatial differences. Here we selected four years (i.e. 1967, 1981, 1994, and 2013) in different decades to display the spatial distributions of crop yield and CWP, as shown in Fig. 11 and Fig. 12. Fig. 11 showed the average crop yield for the eight counties in the four years. Except for the yield in Qilian County, which is less than 2000 kg ha^{-1}, in the other seven counties, the yield was within in the range of 5000–6000 kg ha^{-1}. The maximum yield was in Ganzhou County with 5920 kg ha^{-1}. It was observed from Fig. 11, at the early stage, the high yield area concentrated in the Gaotai and Sunan counties, with crop yield larger than 7000 kg.ha^{-1}, and the crop yield deceased from the western to the eastern. The high-yield area were moving to the eastern part along the time. The crop yield in the Linze and Ganzhou counties increased significantly, with the value larger than 8100 kg ha^{-1} and 9000 kg ha^{-1} respectively. The crop yield in Shandan was also larger than 7700 kg ha^{-1}. While the increase rate of crop yield in Gaotai, Sunan, and Qilian counties was relatively slow.

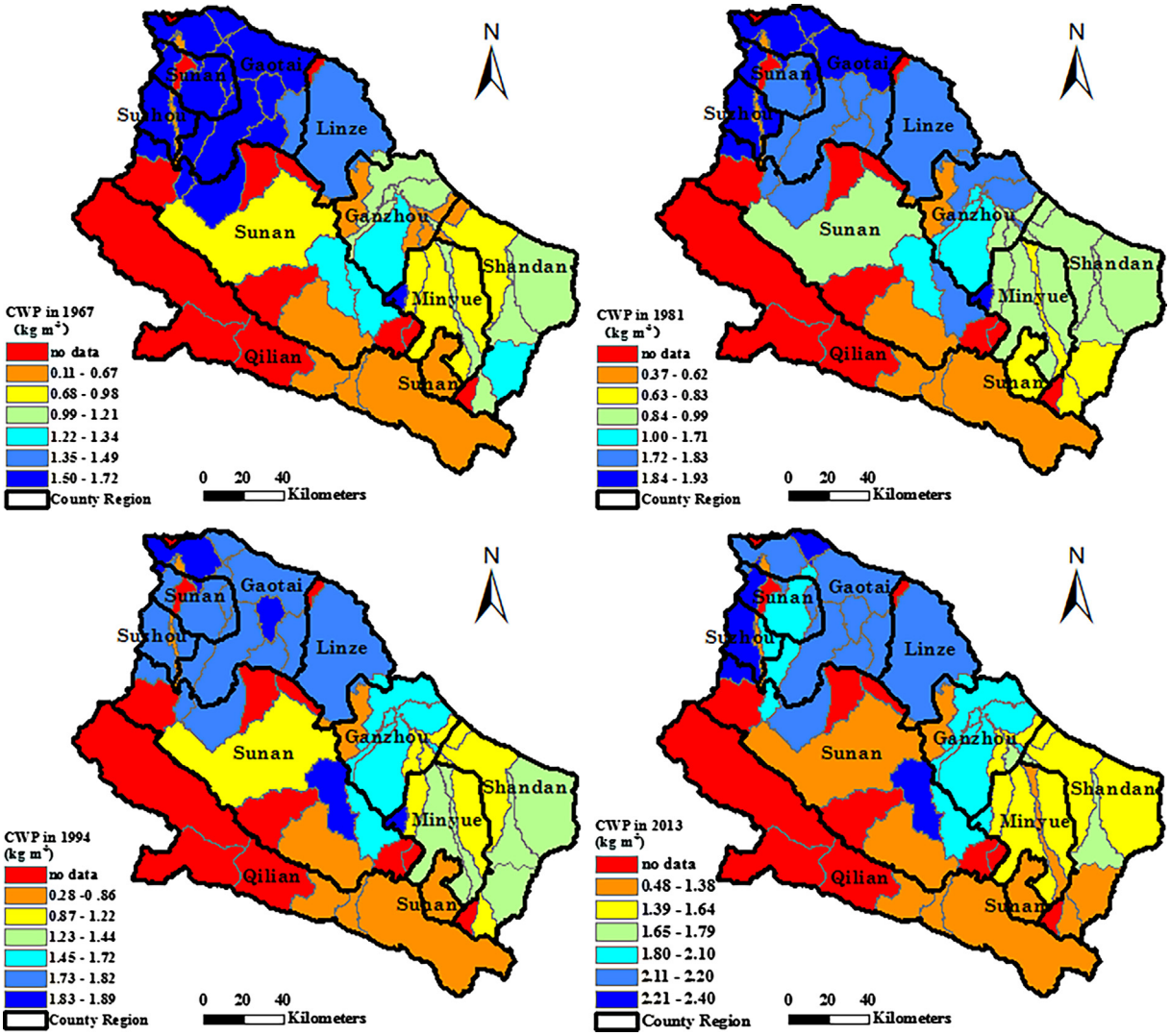

Fig. 12. Same as Fig. 11, but for CWP.

These can be attributed to the following two aspects: (1) In 1960s, the water resources was relatively sufficient, which can meet the crop water requirement for the whole growing season, and the crop yield at that time was mainly controlled by the climate. The heat and light resources are abundant in Gaotai and Sunnan Counties, which resulted in high crop yield during that period. With social-economical development, the water also need to meet the demand of other sectors, and therefore the irrigation water was partly consumed (Ma et al., 2015). The reduction of irrigation water limited the improvement of crop yield. The farmland close to the Yinluoxia station, such as Ganzhou and Linze counties, with sufficient irrigation water, and has improved the crop yield. (2) On the other aspect, for the Qilian and Sunnan Counties, which were located in the upper reaches with relatively lower temperature (Wang et al., 2009), and restricted heat and light resources, the increase rate of crop yield was relatively slower (Zhou et al., 2013).

The spatial distributions of CWP for the upper-middle reaches of the Heihe River basin were shown in Fig. 12. The distribution changes along the time and the patterns were different for those of crop yield in Fig. 11. The high CWP area always concentrated in Gaotai, Suzhou and Linze Counties, and the CWP was growing from 1.5 $kg\,m^{-3}$ to 2.1 $kg\,m^{-3}$. At the early stage in these area, it had relatively high crop-yield. Although the irrigation water was restricted, the irrigation measure and management had been improved. The soil evaporation was reduced, and the regional CWP increasing. Among the eight counties, Ganzou and Linze Counties had high CWP increasing rate, with the improvement about 50–60% for the past four decades. For Minyue and Shandan counties, CWP increased a little of 1.65 $kg\,m^{-3}$. The barley dominated the Minyue and Shandan counties, with the plant area is about 82.6% of the total barely-planting area in the basin. In 1990s, CWP decreased with the RH, and this slowed down the CWP increase rate. In addition, the precipitation in Shandan during the growing season was about 1.6 times to that of the other counties, which will increase the canopy and soil evaporation (Liu, 2012), and in turn lower down the CWP value (Hao, 2015). Therefore, it is suggested that the effective collecting of precipitation in Shandan County, and then a rationally allocation would improve the regional CWP.

4.4. Multi-scale responses of CWP to climatic variation

To reveal the multi-scale responses of CWP to the climatic variations, the wavelet coherence analysis was employed to disclose the co-variability features between them at different time and frequency domains. Fig. 13 showed the local and global coherence of regional CWP over the Ganzhou county in the Heihe River basin with the six meteorological forcing, including precipitation (Prep), solar radiation (SRD), minimum temperature (Tmin), maximum temperature (Tmax), wind speed (WS), and relative humidity (RH). From the local wavelet coherence results (left panel), it was observed that there are more in-

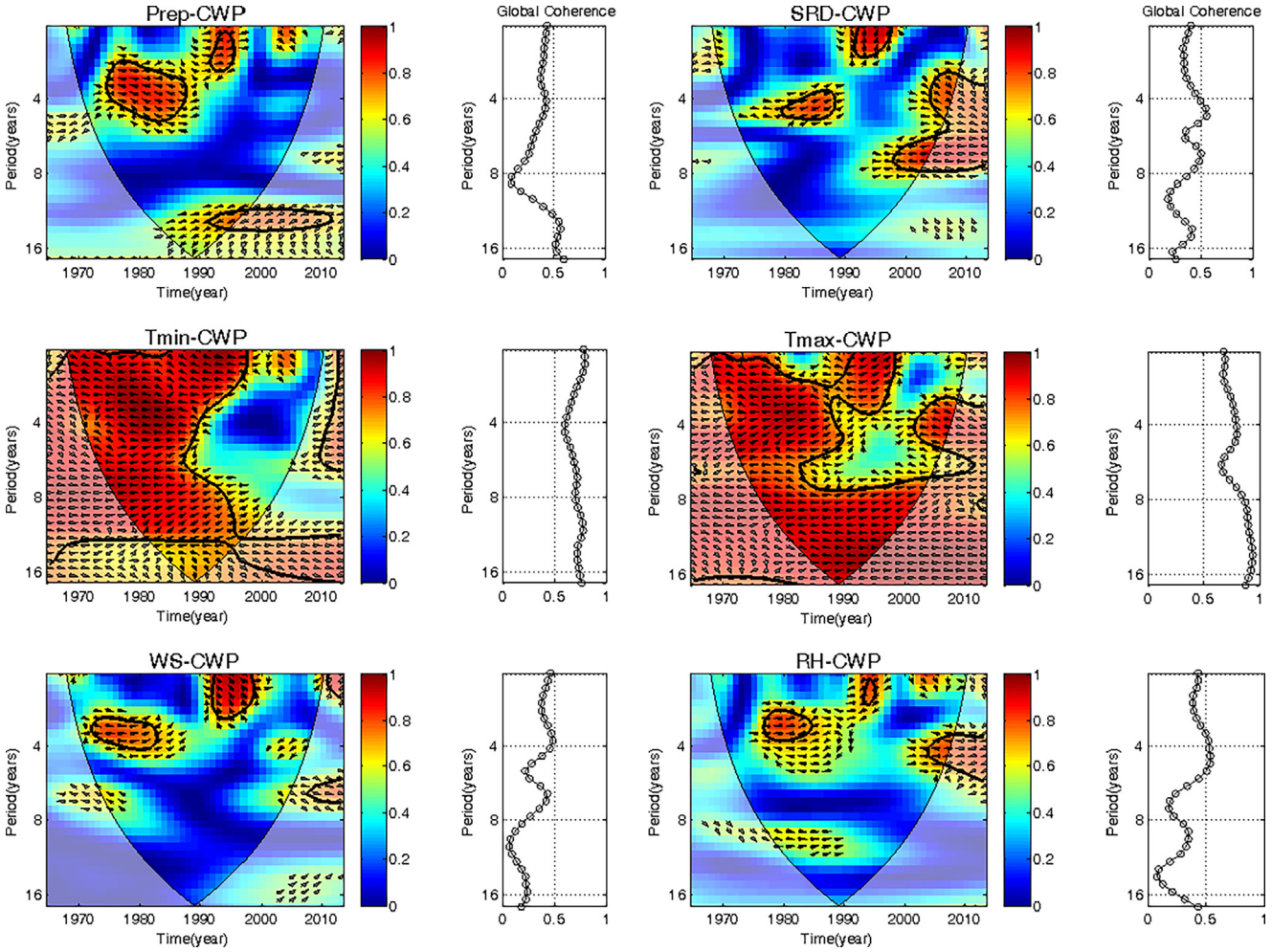

Fig. 13. Wavelet coherence (local and global) between meteorological forcing, including precipitation(Prep), solar radiation (SRD), minimum temperature (Tmin), maximum temperature (Tmax), wind speed (WS), relative humidity (RH), and crop water productivity (CWP) in the Ganzhou county of the Heihe River basin. The 5% significance level against red noise is shown as a thick contour and the cone of influence (COI) where edge effects might become important is shown as a thin black line. The relative phase relationship is shown as arrows (with in-phase pointing right, anti-phase pointing left, meteorological factor leading CWP by 90° pointing straight down, and CWP leading meteorological factor pointing straight up). (For interpretation of the references to colour in this figure legend, the reader is referred to the web version of this article.)

phase relationships between Tmin/Tmax and CWP at both short and relatively longer periods. The global wavelet coherence (right panel) further showed the correlations between Tmax and CWP were basically highest across different timescales, especially at the long-term timescales (e.g. 8–16 years). At the bands of 1–4 year and 4–8 years, the common variability power basically appeared before 2000. The explanations is that, the human activities and irrigation management affected more on the spatial-temporal distributions of CWP in the later period, resulted in a weak control by meteorological forcing. Overall, Tmax showed the most coherence with CWP, which exerted the most meteorological effects on CWP in the upper-middle reaches of the Heihe River basin. For other meteorological variables (Prep, SRD, WS, and RH), the coherence region with high variability power were mainly less than or around 4 year timescales. Moreover, there was little significant coherence between CWP and other variables around 8 year timescales. Therefore, the meteorological variables exerted more effects on the regional CWP at shorter time scales. In addition, the phase relations were also revealed by arrows in Fig. 13. In the significant coherence area, SRD, Tmin, Tmax, and WS mainly showed positive coherence with CWP. The anti-phase relationships can be found between the significant coherence of Prep/RH and that of CWP, which indicated the negative correlations at corresponding timescales.

Fig. 14 summarized the global wavelet coherences between meteorological forcing and CWP for the seven counties, together with the average one for the studied region. In terms of the shorter timescales less than 4 years, Prep, Tmin, WS, and RH showed stronger correlations with CWP in the relatively high-frequency periods. Among it, Tmin in Minyue County displayed a weak correlation with CWP, partly because Minyue County was close to the mountain area and its temperature was relatively lower compared to other counties in the middle reaches of the basin. While the Tmin in Shandan and Linze counties had high coherence with CWP. For the relatively longer timescales than 8 years, the Tmax showed more dominate effects on the CWP evolutions with high global coherence values. The WS in Gaotai and Shandan counties had higher coherence than the average for the long-term timescales.

The elasticities of CWP to six meteorological drivers (RH, Prep, SDR, Tmin, Tmax, and WS) in the Heihe region for three separated periods (1966–1981, 1982–1998, and 1999–2014) were shown in Fig. 15. The elasticity was defined as $\eta(\mathrm{CWP},M_i) = \frac{\Delta CWP / CWP}{\Delta M_i / M_i}$ at annual timescale, where M_i was the different meteorological drivers. It was observed that the elasticity of corn to the climate variables was higher among the four crop types. The elasticities of corn, canola-polish, and wheat all decreased along the three separated periods during 1966–2014. Among it, the decrease rate of corn was the fastest one. This indicated that the major control factors for CWP in the Heihe River basin are changing

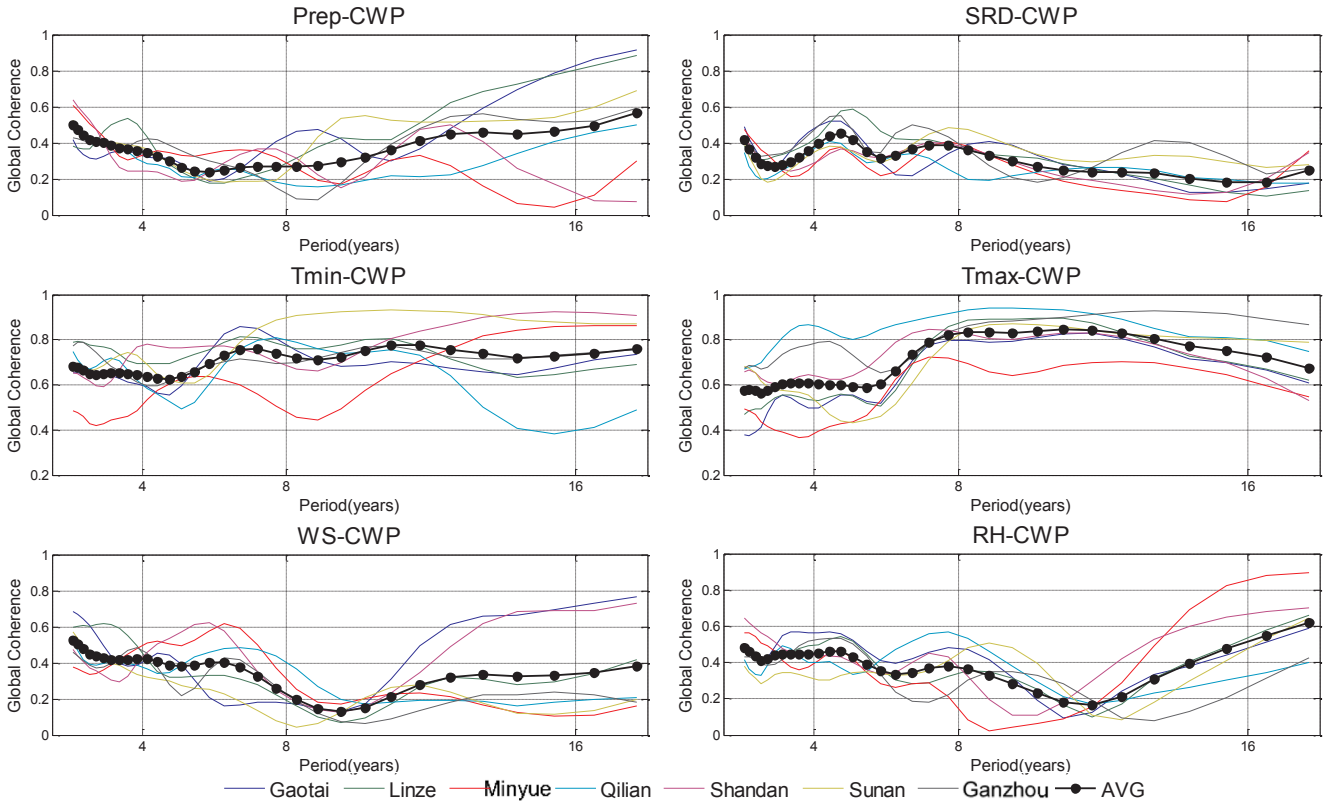

Fig. 14. Global wavelet coherence between meteorological forcing and crop water productivity (CWP) for the seven counties in the Heihe River basin.

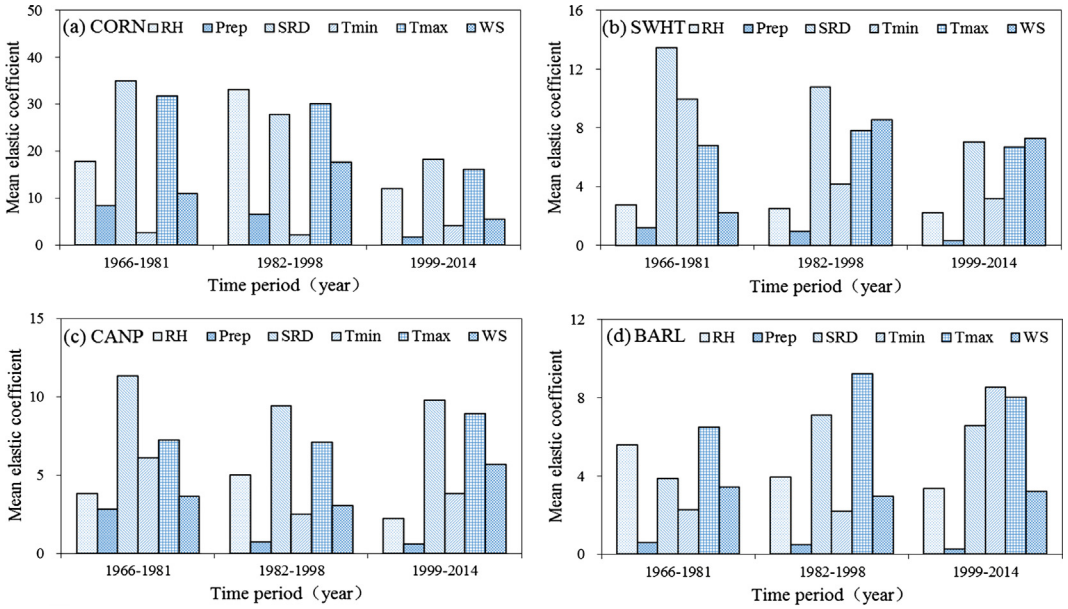

Fig. 15. Elasticities $\eta(CWP, M_i)$ for crop water productivity (CWP), with meteorological forcings M_i taken in turn as precipitation (Prep), solar radiation (SRD), minimum temperature (Tmin), maximum temperature (Tmax), wind speed (WS), relative humidity (RH). (a), (b), (c), and (d) are for spring barley (BARL), spring canola-Polish (CANP), corn (CORN) and spring wheat (SWHT) respectively.

from the single meteorological factors to the combined effects of both climate forcing and human activities (e.g. Zou et al, 2017). The corn was the most important planting crop in the commercial grain base, and it was distributed in many counties. The continuously improved agricultural management and extended scientific technologies improved the corn yield, which resulted in its highest elasticity decrease rate compared with those of other crop types in the region. The elasticity of barley to SRD and Tmax increased in the period of 1982–1998, when compared with the results during 1966–1981. This was partly due to that the responses of CWP to them were relatively higher, and Fig. 8 showed that the average solar radiation and temperature increased during 1982–1998. In addition, the agricultural management for barley was not comparable to corn, especially during the first two periods, and the elasticity was more controlled by the meteorological factors.

5. Conclusions and discussions

The distributed hydrological model of the Heihe River basin in Northwest China was well established using the SWAT model in this study, both for generating runoff in mountainous area and estimating ET in agricultural region with considering irrigation, fertilization and planting patterns. The crop yield and CWP for corn, barley, canola-polish and spring wheat were further simulated for the 49-year period (1966–2014). The spatial-temporal responses of CWP to different meteorological forcing were investigated using wavelet coherence and elasticity analysis. The result will help to improve regional CWP under future changing climate.

The LH-OAT method was firstly employed to examine the sensitivity of model parameters. The observed streamflow in the three gauging stations were used to rank out the first 12 sensitive parameters for the processes of snow-melt, surface runoff, groundwater, soil water, and the river channel routing. Meanwhile, the sensitive parameters of ET processes were identified using the remotely-sensed data. The results show that SFTMP (Snowfall temperature) and CANMX (Maximum canopy index) are the most sensitive parameters in the streamflow and evapotranspiration processes respectively.

Based on the sensitivity results, those parameters were further calibrated for runoff in the mountainous area and ET of the agricultural region in the upper-middle of Heihe River basin, using SUFI-2 method. The simulated monthly streamflow showed a good agreement with the observations at three gauging stations, with the NSE above 0.72 and d_r over 0.73, for both calibration and validation periods during 1966–2000. The ET simulations were calibrated and validated using the remotely-sensed data over 34 sub-basin area, for the periods of 2000–2009 and 2010–2013 respectively. In the validation period, there were 20 sub-basins with the d_r ranged 0.60–0.83 and the NSE above 0.73, which indicated good ET simulation in the Heihe River basin. Moreover, the model parameters on crop yield were calibrated with the observation data from Zhangye Statistic Yearbook for the period of 2005–2014. The results showed the parameters, HVSTI (Harvest index) and CHTMX (Maximum canopy height), are most sensitive parameters to the crop-yield estimation. The crop-yield simulations agree well with the county-based observations for the six counties with MRE lower than 30% and PBAIS close to 0. Overall, the calibrated SWAT model can simulate the hydrologic components and crop growth well for the upper-middle reaches of the Heihe River basin. One limitation is that we did not simulate the detailed processes on the adaptations of crops to climate changes, such as possibly increased root growth in response to drought and delayed phenology in response to temperature changes, which should be improved when investigated at shorter timescales.

The temporal variations of ET, crop yield and CWP were subsequently analyzed for the period 1966–2014. It was found that the ET has an increasing trend with the fluctuations between 401 mm/year and 505 mm/year, which was close to the change of precipitation in the basin. The changing trend of crop yield was different for different crop types. The increasing trend was found for corn and wheat, while the yield of barley showed a decreasing trend. The increasing trend of crop yield mainly corresponded to the change of temperature, especially in the early periods, and the decreasing trend of barely was more related to the decreasing changes of RH in the region. CWP and crop yield are linearly related for the studied period. The average CWP of corn, wheat, and canola-polish are 1.30 kg m^{-3}, 1.00 kg m^{-3}, and 0.48 kg m^{-3} respectively. The average CWP of barely was the largest as 1.45 kg m^{-3}, but showed a slightly decreasing trend. Therefore, expanding the corn planting area will help to improve the regional CWP at current stage.

The spatial distribution of CWP were different due to the variations of planting patterns and climatic background in different counties. The CWP in Linze and Ganzhou were growing all the time, which are above 8100 kg ha^{-1} and 9000 kg ha^{-1} respectively. The following counties in were experiencing increasing trend: Shandan, Minyue, Sunzhou, Gaotai, Sunan, and Qilian counties. Therefore, the center of high CWP region was moved from the west to the east. The barely is a dominated crop in Minye County, and its CWP showed a slowly increasing rate with increasing ET and increasing precipitation. It is suggested that effectively utilizing precipitation would improve the local CWP.

The responses of CWP to six climatic factors were revealed at different scales by wavelet coherence method. Temperature showed the highest coherence with CWP across different timescales. The role of controlling meteorological drivers on CWP at relatively shorter timescales were weak in the later periods when human activities, including fertilization, irrigation, and agricultural management, became insensitive after 1990s. Overall, the Tmax was a major impact factor on the CWP evolution in the Heihe agricultural region.

The SWAT model in the upper-middle reaches of the Heihe River basin was employed to obtain the long-term ET and CWP time series for different counties. The understanding of CWP responses to climatic factors for different crop types provided scientific basis for the sustainable agricultural development, especially under the background of global climate change.

Acknowledgements

This study was supported by the Chinese National Natural Science Foundation Program (51679233, 91425302), and the Special Fund for Agro-scientific Research in the Public Interest (201503125). We thank the two anonymous reviewers for their constructive and valuable comments which resulted in a far more accurate presentation of our work.

References

Abbaspour, K.C., Johnson, C.A., van Genuchten, M.T., 2004. Estimating uncertain flow and transport parameters using a sequential uncertainty fitting procedure. Vadose Zone J. 3, 1340–1352.
Abbaspour, K.C., Yang, J., Maximov, I., Siber, R., Bogner, K., Mieleitner, J., Zobrist, J., Srinivasan, R., 2007. Modelling hydrology and water quality in the pre-alpine/alpine Thur watershed using SWAT. J. Hydrol. 333, 413–430.
Arnold, J.G., Allen, P.M., 1996. Estimating hydrologic budgets for three Illinois watersheds. J. Hydrol. 176, 57–77.
Arnold, J.G., Srinivasan, R., Muttiah, R.S., Williams, J.R., 1998. Large area hydrologic modeling and assessment part I: model development. J. Am. Water Resour. Assoc. 34 (1), 73–89.
Bouman, B.A.M., 2007. A conceptual framework for the improvement of crop water productivity at different spatial scales. Agric. Syst. 93, 43–60.
Cao, L., Dou, Y.X., Zhang, D.Y., 2003. Effect of climate change on ecological environment of Heihe Field. Arid Meteorol. 21 (4), 45–49.
Fang, S.B., 2011. Exploration of method for discrimination between trend crop yield and climatic fluctuant yield. J. Nat. Disasters 20 (6), 13–18.
Faramarzi, M., Yang, H., Schulin, R., Abbaspour, K.C., 2010. Modeling wheat yield and crop water productivity in Iran: implications of agricultural water management for wheat production. Agric. Water Manage. 97, 1861–1875.
Feng, J., 2014. Impact of Climate Change on Water Resources System and Coping Strategies in Heihe River Basin. Donghua University, Shanghai (in Chinese).
Feng, Q., Liu, W., Su, Y.H., Zhang, Y.W., Si, J.H., 2004. Distribution and evolution of water chemistry in Heihe River basin. Environ. Geol. 45, 947–956.
Grinsted, A., Moore, J.C., Jevrejeva, S., 2004. Application of the cross wavelet transform and wavelet coherence to geophysical time series. Nonlinear Process. Geophys. 11, 561–566.
Hao, Y.Y., 2015. Simulation of Irrigated Hydrological Processes and Assessment of Water Productivity in Inner Mongolia Hetao Irrigation District. China Agriculture University, Beijing (in Chinese).
Heilig, G.K., Fishcer, G., Van Velthuizen, H., 2000. Can China feed itself ?—An analysis of China's food prospects with special reference to water resources. Int. J. Sustain. Develop. World Ecol. 7, 153–172.
Immerzeel, W.W., Gaur, A., Zwart, S.J., 2008. Integrating remote sensing and a process-based hydrological model to evaluate water use and productivity in a south Indian catchment. Agric. Water Manage. 95 (1), 11–24.
IPCC, 2014. Climate Change 2014: Impact, Adaptation, and Vulnerability. Cambridge University Press, Cambridge.
Jiang, X., 2014. Study on China's Food Security and the "Three Rural Issues". J. Shanxi Agric. Sci. 42 (8), 771–7859 (in Chinese).
Kijine, J.W., Barker, R., Molden, D., 2003. Water Productivity in Agriculture: Limits and Opportunities for Improvement. CAB International, Wallingford, UK.
Kumar, P., Foufoula-Georgiou, E., 1997. Wavelet analysis for geophysical applications. Rev. Geophys. 35 (4), 385–412.
Lau, K.M., Weng, H.Y., 1995. Climate signal detection using wavelet transform: How to make a time series sing. Bull. Am. Meteorol. Soc. 76, 2391–2402.

Liu, J., Williams, J.R., Zehnder, A.J.B., Yang, H., 2007. GEPIC–modeling wheat yield and crop water productivity with high resolution on a global scale. Agric. Syst. 94, 478–493.
Liu, Z.D., 2012. Utilization of Rainfall and Its Simulation in Winter Wheat. Chinese Academy of Agricultural Sciences, Beijing (in Chinese).
Liu, Z.J., Li, B.P., Li, Y.H., Cui, Y.L., 2004. Research on the water use efficiency and optimal irrigation schedule of the winter wheat. Chin. Soc. Agric. Eng. 20 (4), 58–63.
Luo, Y., He, C., Sophocleous, M., Yin, Z., Ren, H.R., Zhu, O.Y., 2008. Assessment of crop growth and soil water modules in SWAT2000 using extensive field experiment data in an irrigation district of the Yellow River Basin. J. Hydrol. 352, 139–156.
Ma, M.G., Hu, X.L., Wang, J.H., 2015. Ecological and hydrological changes and interactions after recent comprehensive control projects in the Heihe River basin. Terrestrial Atmos. Ocean. Sci. 26 (22), 219–225.
Meng, F.C., Guo, J., Zhou, L., Xiong, M.M., Zhang, L., 2017. Interactive effects of temperature, CO2 concentration and precipitation on growth and yield of crops. Chin. J. Appl. Ecol. 28 (12), 1–12.
Monteith, J.L., 1965. Evaporation and the environment. Symp. Soc. Experim. Biol. 19, 205–234.
Neitsch, S.L., Arnold, J.G., Kiniry, J.R., Williams, J.R., 2005. Soil and Water Assessment Tool, Theoretical Documentation: Version 2005. Grassland, Soil and Water Research Laboratory, Agricultural Research Service and Blackland Research Center: Texas Agricultural Experiment Station, Temple, Tex.
Nguyen, V.T.V., Desramaut, N., Nguyen, T.D., 2010. Optimal rainfall temporal patterns for urban drainage design in the context of climate change. Water Sci. Technol. 62 (5), 1170–1176.
Niu, J., Kang, S.Z., Zhang, X.T., Fu, J., 2017. Vulnerability analysis based on drought and vegetation dynamics. Ecol. Ind. http://dx.doi.org/10.1016/j.ecolind.2017.10.048.
Sacks, W.J., Kucharik, C.J., 2011. Crop management and phenology trends in the US Corn Belt: Impacts on yields, evapotranspiration and energy balance. Agric. For. Meteorol. 633, 220–229.
Saeijs, H.L., van Berkel, M.J., 1995. Global water crisis: the major issue of the 21st century, a growing and explosive problem. Eur. Water Pollut. Control 5 (4), 26–40.
Schuol, J., Abbaspour, K.C., Yang, H., Srinivasan, R., Zehnder, A.J.B., 2008. Modeling blue and green water availability in Africa. Water Resour. Res. 44, W07406. http://dx.doi.org/10.1029/2007WR006609.
Setegn, S.G., Srinivasan, R., Melesse, A.M., Dargahi, B., 2010. SWAT model application and prediction uncertainty analysis in the Lake Tana Basin, Ethiopia. Hydrol. Process. 24, 357–367.
Siebert, S., Doll, P., 2010. Quantifying blue and green virtual water contents in global crop production as well as potential production losses without irrigation. J. Hydrol. 384 (3–4), 198–217.
Singh, R., Kroes, J.G., van Dam, J.C., Feddes, R.A., 2006. Distributed ecohydrological modelling to evaluate the performance of irrigation system in Sirsa district, India: I. Current water management and its productivity. J. Hydrol. 329, 692–713.
Sivakumar, B., 2011. Global climate change and its impacts on water resources planning and management: assessment and challenges. Stochastic Environ. Res. Risk Assess. 25, 583–600.
Sloan, P.G., Moore, I.D., Coltharp, G.B., Eigel, J.D., 1983. Modeling surface and subsurface stormflow on steeply-sloping forested watersheds. Water Resources Institute Report 142. University of Kentucky, Lexington, Kentucky.
Sun, C., Ren, L., 2014. Assessing crop yield and crop water productivity and optimizing irrigation scheduling of winter wheat and summer maize in the Haihe plain using SWAT model. Hydrol. Process. 28, 2478–2498.
Torrence, C., Compo, G.P., 1998. A practical guide to wavelet analysis. Bull. Am. Meteorol. Soc. 79 (1), 62–78.
Torrence, C., Webster, P.J., 1999. Interdecadal changes in the ENSO-Monsoon system. J. Clim. 12, 2679–2690.
USDA Soil Conservation Service, 1972. National Engineering Handbook, Section 4 Hydrology. USDA, Washington DC.
van Griensven, A., Meixner, T., Grunwald, S., Bishop, T., Diluzio, M., Srinivasan, R., 2006. A global sensitivity analysis tool for the parameters of multi-variable catchment models. J. Hydrol. 324, 10–23.
Wallace, J.S., Gregory, P.J., 2002. Water resources and their use in food production systems. Aquat. Sci. 64, 363–375.
Wang, H.J., Zhang, B., Jin, X.H., Zhang, H., Liu, J.F., Dai, S.P., 2009a. Spatio-temporal variations analysis of air temperature and precipitation in qilian mountainous region based on GIS. J. Desert Res. 29 (6), 1196–1202.
Wang, H.L., Zhang, Q., Wang, R.Y., Lv, X.D., Wang, L., Zhang, L., Qi, Y., 2017a. Effects of climate change on agro climatic resources and potential primary cropping patterns in Gansu Province. Acta Ecol. Sin. 37 (18), 6099–6110.
Wang, J.X., Li, R.Y., Huang, J.K., Yan, T.T., Sun, T.H., 2017b. Growing water scarcity, food security and government responses in China. Glob. Food Secur. 14 (2017), 9–17.
Wang, L.C., Zhang, X.Y., 2010. Effect of the recent climate change on water resource in Heihe river basin. J. Arid Land Resour. Environ. 24 (4), 60–65.
Wang, G.S., Xia, J., Chen, J., 2009b. Quantification of effects of climate variations and human activities on runoff by a monthly water balance model: a case study of the Chaobai River basin in northern China. Water Resour. Res. 45 (7), W00A11. http://dx.doi.org/10.1029/2007WR006768.
Wen, D.P., Li, J., He, P.F., 2017. Grey correlation analysis of agro-meteorological disasters and soybean yield in Heilongjiang province. J. Nat. Disasters 26 (4), 56–62.
Williams, J.R., Jones, C.A., Dyke, P.T., 1984. A modeling approach to determining the relationship between erosion and soil productivity. Trans. ASAE 27, 129–144.
Willmott, C.J., Robeson, S.M., Matsuura, K., 2011. Short communication A refined index of model performance. Int. J. Climatol. 32, 2088–2094.
Wu, Y.P., Liu, S.G., Abdul-Aziz, O.I., 2012. Hydrological effects of the increased CO2 and climate change in the Upper Mississippi River basin using a modified SWAT. Clim. Change 110, 977–1003.
Xue, J., Ren, L., 2017. Assessing water productivity in the Hetao Irrigation District in Inner Mongolia by an agro-hydrological model. Irrigat. Sci. 35 (4), 357–382.
Yang, L.S., Feng, Q., Yin, Z.L., Wen, X.H., Si, J.H., Li, C.B., Deo, R.C., 2017. Identifying separate impacts of climate and land use/cover change on hydrological processes in upper stream of Heihe River, Northwest China. Hydrol. Process. 31 (5), 1100–1112.
Zhang, A.J., Liu, W.B., Yin, Z.L., Fu, G.B., Zheng, C.M., 2016. How will climate change affect the water availability in the Heihe River Basin, Northwest China? J. Hydrometeorol. 17 (5), 1517–1542.
Zhang, G.H., Nie, Z.L., Liu, S.Y., Wang, J.Z., 2006. Threshold of influence of water resources in the Heihe River valley, northwestern Gansu. Geol. Bull. China 25 (1–2), 244–250.
Zhang, H.P., Oweis, T., 1999. Water-yield relations and optimal irrigation scheduling of wheat in the Mediterranean region. Agric. Water Manage. 38 (3), 195–211.
Zhang, J., Li, D.L., 2004. Analysis on distribution character of rainfall over Qilian mountain and Heihe valley. Plateau Meteorol. 23 (1), 81–88.
Zhao, J.F., Guo, J.P., Zhang, Y.H., Xu, J.W., 2010. Advance in research of impacts of climate change on agriculture. Chin. J. Agrometeorol. 31 (2), 200–205.
Zhang, K., et al., 2015. Vegetation greening and climate change promote multidecadal rises of global land evapotranspiration. Sci. Rep. 5, 15956. http://dx.doi.org/10.1038/srep15956.
Zhou, G.X., Zhang, G.L., Dai, H.Y., Li, J., 2013. Influence of light/heat resources change during crop growing seasons on agricultural production in West Liaoning. J. Shanxi Agric. Sci. 41 (9), 955–958.
Zhou, W.K., 2012. Ph.D. thesis In: Impact of Climate Change Impact on Chinese Food Production and its Countermeasures. Nanjing Agricultural University, Nanjing, pp. 165 (in Chinese).
Zou, M.Z., Niu, J., Kang, S.Z., Li, X.L., Lu, H.L., 2017. The contribution of human agricultural activities to increasing evapotranspiration is significantly greater than climate change effect over Heihe agricultural region. Sci. Rep. 7, 8805. http://dx.doi.org/10.1038/s41598-017-08952-5.